REPORT DOCUMENTATION PAGE

Form Approved OMB NO. 0704-0188

1. REPORT DATE (DD-MM-YYYY)	2. REPORT TYPE	3. DATES COVERED (From - To)
31-03-2009	Final Report	26-Sep-2005 - 31-Dec-2008

4. TITLE AND SUBTITLE

A NEW PARADIGM IN MODELING AND SIMULATIONS OF COMPLEX OXIDATION CHEMISTRY USING A STATISTICAL APPROACH

5a. CONTRACT NUMBER
W911NF-05-1-0526

5b. GRANT NUMBER

5c. PROGRAM ELEMENT NUMBER
611102

6. AUTHORS
Josette Bellan

5d. PROJECT NUMBER

5e. TASK NUMBER

5f. WORK UNIT NUMBER

7. PERFORMING ORGANIZATION NAMES AND ADDRESSES
California Institute of Technology
Sponsored Research MC 201-15
California Institute of Technology
Pasadena, CA 91125 -

8. PERFORMING ORGANIZATION REPORT NUMBER

9. SPONSORING/MONITORING AGENCY NAME(S) AND ADDRESS(ES)
U.S. Army Research Office
P.O. Box 12211
Research Triangle Park, NC 27709-2211

10. SPONSOR/MONITOR'S ACRONYM(S)
ARO

11. SPONSOR/MONITOR'S REPORT NUMBER(S)
48308-EG.5

12. DISTRIBUTION AVAILIBILITY STATEMENT
Approved for public release; federal purpose rights

13. SUPPLEMENTARY NOTES
The views, opinions and/or findings contained in this report are those of the author(s) and should not contrued as an official Department of the Army position, policy or decision, unless so designated by other documentation.

14. ABSTRACT

This report describes a study performed under ARO sponsorship, addressing the investigation of a novel way to reduce complex and extensive oxidation reaction mechanisms containing hundreds of species to a much smaller number of progress variables, typically by a factor of ten. Because the results have been documented in several manuscripts, this final report is in the form of an Executive Summary succinctly describing the results and putting them in perspective with respect to existing oxidation mechanism reduction schemes. The manuscripts are

15. SUBJECT TERMS
reduced chemical kinetic mechanisms

16. SECURITY CLASSIFICATION OF:			17. LIMITATION OF ABSTRACT	15. NUMBER OF PAGES	19a. NAME OF RESPONSIBLE PERSON
a. REPORT	b. ABSTRACT	c. THIS PAGE			Josette Bellan
U	U	U	SAR		19b. TELEPHONE NUMBER 818-354-6959

Report Title

A NEW PARADIGM IN MODELING AND SIMULATIONS OF COMPLEX OXIDATION CHEMISTRY USING A STATISTICAL APPROACH

ABSTRACT

This report describes a study performed under ARO sponsorship, addressing the investigation of a novel way to reduce complex and extensive oxidation reaction mechanisms containing hundreds of species to a much smaller number of progress variables, typically by a factor of ten. Because the results have been documented in several manuscripts, this final report is in the form of an Executive Summary succinctly describing the results and putting them in perspective with respect to existing oxidation mechanism reduction schemes. The manuscripts are individually listed as Appendices, and attached to this report.

List of papers submitted or published that acknowledge ARO support during this reporting period. List the papers, including journal references, in the following categories:

(a) Papers published in peer-reviewed journals (N/A for none)

The study involved a change of paradigm, and the study is not mature yet for a comprehensive journal publication.

Number of Papers published in peer-reviewed journals: 0.00

(b) Papers published in non-peer-reviewed journals or in conference proceedings (N/A for none)

Number of Papers published in non peer-reviewed journals: 0.00

(c) Presentations

1. “A new method in modeling and simulations of complex oxidation chemistry”, (K. G. Harstad and J. Bellan), AIAA 2007-1433, presented at the 45th Aerospace Sciences Meeting, Reno, NV, January 8-11, 2007; also paper C10 at the 5th Joint Sections Meeting of the Combustion Institute, San Diego, CA, March 26-28, 2007
2. “A Simplified Model of Alkane Oxidation”, (K. G. Harstad and J. Bellan), AIAA 2008-0975, presented at the 46th Aerospace Sciences Meeting, Reno, NV, January 7-10, 2008
3. “Computationally efficient modeling of n-heptane oxidation using constituents and species”, (K. G. Harstad and J. Bellan), 32nd Symposium Int. on Combustion, Montreal, Canada, August 3-8, 2008
4. “Modeling of Alkane Oxidation using Constituents and Species”, (K. G. Harstad and J. Bellan), AIAA-2009-1368, presented at the 47th Aerospace Sciences Meeting, Orlando, FL, January 5-8, 2009; also paper 13G4 to be presented at the 6th US National Combustion Meeting, Ann Arbor, Michigan, May 17-20, 2009

Number of Presentations: 4.00

Non Peer-Reviewed Conference Proceeding publications (other than abstracts):

Number of Non Peer-Reviewed Conference Proceeding publications (other than abstracts): 0

Peer-Reviewed Conference Proceeding publications (other than abstracts):

“Computationally efficient modeling of n-heptane oxidation using constituents and species”, (K. G. Harstad and J. Bellan), 32nd Symposium Int. on Combustion, Montreal, Canada, August 3-8, 2008

Number of Peer-Reviewed Conference Proceeding publications (other than abstracts): 1

(d) Manuscripts

None yet. The study is not yet at the proper stage of maturity.

Number of Manuscripts: 0.00

Number of Inventions:

Graduate Students

NAME	PERCENT_SUPPORTED
FTE Equivalent:	
Total Number:	

Names of Post Doctorates

NAME	PERCENT_SUPPORTED
FTE Equivalent:	
Total Number:	

Names of Faculty Supported

NAME	PERCENT_SUPPORTED	National Academy Member
Josette Bellan	0.04	No
FTE Equivalent:	**0.04**	
Total Number:	**1**	

Names of Under Graduate students supported

NAME	PERCENT_SUPPORTED
FTE Equivalent:	
Total Number:	

Student Metrics

This section only applies to graduating undergraduates supported by this agreement in this reporting period

The number of undergraduates funded by this agreement who graduated during this period:	0.00
The number of undergraduates funded by this agreement who graduated during this period with a degree in science, mathematics, engineering, or technology fields:.....	0.00
The number of undergraduates funded by your agreement who graduated during this period and will continue to pursue a graduate or Ph.D. degree in science, mathematics, engineering, or technology fields:.....	0.00
Number of graduating undergraduates who achieved a 3.5 GPA to 4.0 (4.0 max scale):	0.00
Number of graduating undergraduates funded by a DoD funded Center of Excellence grant for Education, Research and Engineering:	0.00
The number of undergraduates funded by your agreement who graduated during this period and intend to work for the Department of Defense	0.00
The number of undergraduates funded by your agreement who graduated during this period and will receive scholarships or fellowships for further studies in science, mathematics, engineering or technology fields:	0.00

Names of Personnel receiving masters degrees

NAME
Total Number:

Names of personnel receiving PHDs

NAME
Total Number:

Names of other research staff

NAME	PERCENT_SUPPORTED	
Dr. Kenneth Harstad	0.38	No
FTE Equivalent:	**0.38**	
Total Number:	**1**	

Sub Contractors (DD882)

Inventions (DD882)

FINAL REPORT

A NEW PARADIGM IN MODELING AND SIMULATIONS OF COMPLEX OXIDATION CHEMISTRY USING A STATISTICAL APPROACH

Josette Bellan
California Institute of Technology
Mechanical Engineering Department
Pasadena CA 91125

Abstract

This report describes a study performed under ARO sponsorship, addressing the investigation of a novel way to reduce complex and extensive oxidation reaction mechanisms containing hundreds of species to a much smaller number of progress variables, typically by a factor of ten. Because the results have been documented in several manuscripts, this final report is in the form of an Executive Summary succinctly describing the results and putting them in perspective with respect to existing oxidation mechanism reduction schemes. The manuscripts are individually listed as Appendices, and attached to this report.

TABLE OF CONTENTS

.

EXECUTIVE SUMMARY

The highlights of the results from the manuscripts in Appendices 1-4 are here summarized.

The challenge of modeling turbulent reactive flows is so considerable that the activity has traditionally been decomposed into its two essential parts: kinetics and turbulence. Usually, modeling of chemical kinetics has proceeded on a separate path from that of turbulence which also includes canonical models for turbulence/reaction interaction. The only constraint to kinetic modeling was that it should be compact enough to be computationally efficient when included in a complex turbulent combustion code. However, there are definite advantages on approaching chemical kinetic modeling in a similar manner to turbulent flow modeling because if the concepts are similar, the hope is that the models will mesh better and the results will be easier to understand. This was the approach taken in this study. The spirit of the chemical kinetic modeling approach is that of Large Eddy Simulations (LES) in which kinematically energetically-significant flow scales are computed and the others are modeled; in turbulence, the large flow scales constitute the former category and the small flow scales constitute the latter category. The chemical kinetics parallel is to obtain a model in which one retains only the thermodynamically energetically-significant chemical scales as progress variables, and models the fate of the other scales. But the parallel approach between kinetics and turbulence was extended even further. In turbulence modeling, a common methodology is to assess the behavior of the modeled scales by analyzing databases created using Direct Numerical Simulations (DNS) in which all flow scales are computed; indeed, current experimental diagnostics do not permit the same thoroughness of information as that obtained from DNS. The DNS data is analyzed in what is called an *a priori* study to inquire about the behavior of the small scales and propose mathematical forms which fit this behavior. The *a priori* study is followed by an *a posteriori* study where the proposed mathematical forms are inserted into the model to evaluate its performance when compared to the DNS database at the LES resolution.

A complete analogy between turbulence and kinetics was made by observing that kinetic elemental or skeletal mechanisms can serve for reduced kinetics the role that DNS serves for LES, in which case reduced kinetic mechanisms can be viewed as the complement to LES in achieving the goal of accurate computationally-efficient turbulent reactive flow simulations. The analogy between reduced kinetic models and LES is not entirely surprising since each chemical species has a characteristic time scale and in the kinetic reduction it is desirable to compute only those entities (e.g. species, combination of species, radicals, combination of radicals, etc.) having essential characteristic time scales (to be defined) and model the kinetics of the remaining entities.

Thus, there were two important components to this study, namely the *a priori* analysis and the *a posteriori* evaluation. Whereas turbulence modeling benefits from decades of work using the DNS/LES concept which originated in atmospheric turbulence predictions in the 1960s, the present work is the first investigation to take this approach in kinetic reduction modeling. Therefore, it was first necessary to produce a categorization of scales analogous to the large and small scales of turbulence, then it was required to propose mathematical forms for the scales that

will be modeled rather than computed as progress variables in the reduced kinetic model, and finally it was required to perform an *a posteriori* study in order to evaluate the chemical kinetic model versus the elemental or skeletal mechanism for those species predicted by the reduced model. The present model depicts a constant-volume situation, so as to be consistent with the requirement of a LES grid.

We have proposed such a categorization [1-4] through the definition of a total constituent molar density which is a progress variable representing the heavy species kinetics, and through the partition of the light species set into a set of modeled quasi-steady species and a set of progress variable species. By definition, constituent radicals are those composing species with a carbon number larger than or equal to 3. These species are called 'heavy', and their complement in the ensemble of species is called 'light'. The total constituent molar density is the sum of the individual constituents' molar densities. Thus, rather than following all species through their reaction coordinates, we follow a reduced set of reaction coordinates (i.e. progress variables); this reduced set is called a base. The *a priori* model, with numerous results was described in [1-4]. The behavior of the base set was examined *a priori* in the context of a detailed reaction model for n-heptane combustion as given by LLNL [5], and the proposed mathematical forms were tested against the LLNL kinetic scheme. The first *a posteriori* evaluation of the model was presented in [4] with the goal of inquiring whether the qualitative aspects of the reaction evolution were captured and identifying refinements that could be made to improve, if necessary, the quantitative agreement with the LLNL database.

To give perspective to our model, one must consider that there are several ways of simplifying the chemistry, but the terminology employed for qualifying this simplification is not unified and instead depends on the author. For example, in [6] the 'complete mechanism' is denoted as that in which all kinetic processes have been taken into account; a 'detailed' or 'skeletal' mechanism is that where the complexity of the complete mechanism has been reduced for a given purpose, while keeping all main kinetic pathways important for the situation at hand (reactions considered unimportant through sensitivity analysis are eliminated and possibly lumping of isomers decreases the number of species, and thus decreases the number of differential equations); a 'semi-global' mechanism is defined as that involving 5-10 species and in which most chemical pathways have been neglected; and a 'single-step' mechanism is that where all intermediary species have been removed and only reactants and products appear. The authors of [6] acknowledge that the boundaries between defined categories are not rigid. According to their definition, the skeletal mechanism represents the lower limit of the detailed mechanism. Another frequent terminology in kinetic modeling is that of a 'reduced' mechanism, meaning that the mechanism is smaller than the original one. For example, there is a large number of smaller-than-the-LLNL-mechanism for n-heptane, from that of [7] that is a 30-step mechanism, to that of [8] having a set of 14 reactions and 16 species, to that further adjusted in [9] to a set of 4 steps and 5 species. Recently, researchers have announced [10] a new n-heptane skeletal mechanism of 78 species with 359 or 317 reactions, another skeletal mechanism with 68 species and 283 reactions, and a reduced mechanism with 55 species and 51 global steps (i.e. which can be selected from either elementary or lumped reactions, their rate expressions being the linear combination of the rates of the elementary reactions.). This means that the minimum number of progress variables, that is, the number of variables for which differential equations are

solved, is 55. A remaining number of 13 species is determined using algebraic equations by invoking the quasi-steady state assumption. All these mechanisms were tested in the range of 1atm to 50atm for the pressure, 600K to 1800K for the ignition temperature, and 0.5 to 1.5 for the equivalence ratio; testing involved comparisons with the full kinetic mechanism [5], and also with flame data.

There are several kinetic mechanism methodologies which can be generally classified as either 'fixed' or 'on-the-fly'. In fixed methodologies, the kinetic mechanism is smaller than the original one and when entering a reaction calculation the same mechanism is meant to be used during the entire calculation. An example of a fixed mechanism is given in [10]. In contrast, for 'on-the-fly' mechanisms, criteria are used to sample during a reaction calculation the entire mechanism, and at each time a reduction is found, which may vary during the calculation. An example of such a method is that of the intrinsic low-dimensional manifold (ILDM) [11]. The ILDM method is based on the observation that in a chemically reactive mixture at constant pressure, constant enthalpy and constant element composition, the path of reaction in the high-dimensional state space lies in low-dimensional manifolds far from the final equilibrium point; these manifolds are intrinsic, meaning that except for the degree of reduction, the reaction mechanism in terms of Arrhenius-type elementary reactions is the only source of information necessary to build the approximation. It was found [11] that ILDM is not easily implementable in some situations. Particularly, it (i) has the drawback of becoming very difficult to handle with increasing number of C atoms in the fuel [11], and we note that heavy species (i.e. large number of C atoms) enter the composition of most practical fuels, and (ii) does not work at low temperatures (the ignition region), or very lean or rich mixture conditions, which are precisely the conditions where a very large number of pollutants are formed.

In our methodology [1-4], a much larger reduction than that obtained in [10] has been achieved because instead of the 55 progress variables based on species, as in [10], we only have only 12 progress variables based on constituent radicals and light species, as defined below. Moreover, instead of the n-heptane mechanism being only valid in the range of 1atm to 50atm, 600K to 1800K and 0.5 to 1.5 for the equivalence ratio, our range is 5bar to 60bar, temperatures as low as 600K and as high as 2500K depending on the pressure, and 0.125 to 8 range for the equivalence ratio. The slightly higher pressure is helpful for diesel, gas turbine and HCCI engines; the higher temperature at the upper limit is important for NO_x production reactions to be grafted on the present mechanism in future work; the considerably wider equivalence ratio regime is crucial for NO_x production in the lean regime and CO and soot production in the rich regime (future work).

Moreover, our model is hierarchical by construct, meaning that it is naturally extendable to higher carbon-number hydrocarbons (a primary necessity for modeling iso-octane and ring hydrocarbons), thus having advantages in this respect over the capabilities of ILDM. The hierarchical aspect comes in because the progress variables are not necessarily species, but also include species 'constituents' [1-4], defined very much like in group additivity theory [12]. In contrast to groups [12], constituents take into account only interactions with adjacent groups and only first order (compositional) effects. Examination of the LLNL n-heptane mechanism over a wide range of pressures and stoichiometries showed that most of the constituent rates are quasi-

steady; exceptions are only for radicals with minor contribution to the total. Our modeling effort reduced the LLNL n-heptane mechanism from 160 species (progress variables) and 1540 reactions to 12 progress variables (11 light species and the global constituent mole fraction) for which 16 rates (the contributions of the heavy species to the light species -11 gain rates and 4 loss rates- and the global constituent rate) have been modeled by fitting, 162 conventional reaction rates (light species interacting among themselves) and 11 other functional forms (i.e. fits for the heat capacity at constant pressure, the enthalpy release rate of the heavy species, and the molar fraction of quasi-steady light species). The reduced model comprises 16 rate functions, 11 curves for light quasi-steady mole fractions and the heat capacities of the heavies fitted in terms of a normalized temperature, the stoichiometric ratio, the initial temperature, and an initial scaled pressure parameter. This is a reduction of the number of progress variables by an order of magnitude from the LLNL elementary mechanism. This compact model was verified by comparing temperature evolution paths from calculations using the LLNL dataset to corresponding paths from the reduced model of constituents and light species; deviations were at most a few percent. Therefore, going from n-heptane to heavier hydrocarbons the number of constituents may increase (e.g. with aromatics), but if as for n-heptane they can all be bundled into a single total constituent mole fraction that is the single representative progress variable of the constituents, it is predicted that the computational time should remain essentially the same.

The detailed analysis of the database had an additional advantage: the finding of a scaling of the global constituents mole fraction and of a temperature non-dimensional variable that allowed the establishment of a self-similarity of the global constituents' mole fraction with respect to the non-dimensionalized temperature, pressure, equivalence ratio and temperature at which the global constituents reaction rate becomes positive [4]. This self similarity is a reduction in problem dimensionality but is not to be confused with ILDM which was for species, whereas the present one is for the constituents. The fact that the constituents can embody the evolution of the heavy species is physically consistent with the fact that as the temperature increases, the heavy species decompose and no longer play a role; instead, the products of this decomposition determine the reaction evolution.

Finally, the preliminary *a posteriori* study revealed that the qualitative features of the reaction evolution are well captured but that fitting of the reaction rates in the initial part of the incubation region (where the non-dimensional temperature is smaller than 10^{-2}) must be improved to obtain good quantitative results. In this region, the temperature increases by approximately 5K (we call this the quiescent part of the incubation region), before the reaction transitions to the next part of the incubation region (which we call the active part) where the temperature increases to approximately 1000K which results in the alteration of the heavy species structure and brings about their decomposition. This improved fitting has been performed and is currently being evaluated *a posteriori* in the renewed grant from ARO on this subject.

REFERENCES

[1] Harstad, K. G. and Bellan, J., "A new method in modeling and simulations of complex oxidation chemistry", AIAA 2007-1433, presented at the 45th Aerospace Sciences Meeting, Reno, NV, January 8-11, 2007; also paper C10 at the 5th Joint Sections Meeting of the Combustion Institute, San Diego, CA, March 26-28, 2007

[2] Harstad, K. G. and Bellan, J., "A Simplified Model of Alkane Oxidation", AIAA 2008-0975, presented at the 46th Aerospace Sciences Meeting, Reno, NV, January 7-10, 2008

[3] Harstad, K. G. and Bellan, J., "Computationally efficient modeling of n-heptane oxidation using constituents and species", 32nd Symposium Int. on Combustion, Montreal, Canada, August 3-8, 2008

[4] Harstad, K. G. and Bellan, J., "Modeling of Alkane Oxidation using Constituents and Species", AIAA-2009-1368, presented at the 47th Aerospace Sciences Meeting, Orlando, FL, January 5-8, 2009; also paper 13G4 to be presented at the 6th US National Combustion Meeting, Ann Arbor, Michigan, May 17-20, 2009

[5] Lawrence Livermore National Laboratory, http://www-cms.llnl.gov/combustion/combustion2.html.

[6] Hilbert, R., Tap, F., El-Rabii, H and Thévenin, D., Impact of detailed chemistry and transport models on turbulent combustion simulations, *Progress in Energy and Combustion Sciences*, 30, 61-117, 2004

[7] Peters, N., Paczko, G., Seiser, R. and Seshadri, K., *Combust. Flame*, Temperature cross-over and non-thermal runaway at two-stage ignition of n-heptane, 128(1-2), 38-59, 2002

[8] Pitsch, H. and Peters, N., Investigation of the ignition process of sprays under diesel engine conditions using reduced n-heptane chemistry, SAE paper 982464, 1998

[9] Müeller, U. C., Peters, N. and Linan, A., Global kinetics for n-heptane ignition at high pressures, *Proc. Symp. Inst*., 24, 777-784, 1992

[10] Lu, T. and Law, C. K., Strategies for mechanism reduction for large hydrocarbons: n-heptane, paper C21, 5th Us Combustion Meeting, San Diego, CA., March 25-28, 2007

[11] Correa, C., Niemann, H., Schramm, B. and Warnatz, J., Reaction mechanism reduction for higher hydrocarbons by the ILDM method, *Proc. Combust. Inst.*, 28, 1607-1614, 2000

[12] Benson, S. W., *Thermochemical Kinetics*, John Wiley & Sons, Inc., 1968

APPENDIX 1

A new method in modeling and simulations of complex oxidation chemistry

Kenneth G. Harstad[**,*] and Josette Bellan[♦,**,†]
California Institute of Technology[♦], *Pasadena, CA 91125*
Jet Propulsion Laboratory[**], *California Institute of Technology,*
Pasadena CA 91109-8099

A simplified model is proposed for the kinetics of alkane oxidation in air, based on a decomposition of heavy (carbon number ≥ 3) hydrocarbons into a 13 constituent radical base. The behavior of this base is examined in test computations for heptane utilizing Chemkin II with LLNL data inputs. Emphasis is placed on prediction of the heat release and temperature evolution. At stoichiometric conditions, the total constituent molar density was found to follow a quasi-steady rate which is a simplification in the modeling of its reaction rate.

Introduction

Computational models for turbulent reactive flows present challenges that have yet to be fully met. First, combustion of typical hydrocarbons proceeds through the formation of hundreds of species interacting through thousands of reactions. Second, a complete numerical resolution of high Reynolds number flow requires a very large number of grid points that is beyond current typical supercomputer capabilities. Thus, combining detailed reaction rate models with the fundamental flow equations yields a computational problem that is computationally prohibitive. A drastic (at least order of magnitude) reduction in the dimension of reaction kinetics is required for a feasible computational model. In spirit, this reduction is similar to that to be achieved in Large Eddy Simulations (where energetically significant flow scales are computed and the others are modeled) with respect to Direct Numerical Simulations (where all flow scales are computed). Since each species has a characteristic time scale, in the kinetic reduction it is also desirable to compute only those species that have an essential characteristic time scale (in a sense to be defined) and model the kinetics of the remaining species.

We categorize all species involved in hydrocarbon oxidation into light species and heavy species; the heavy species are those having a carbon number $n \geqslant 3$. Based on this definition, a method for simplifying alkane combustion is proposed that focusses on a small set of constituent radicals (concept to be defined in Section I) of the heavy species rather than on the much larger number of these species. That is, rather than following all species through their reaction coordinates, we will follow a reduced set of reaction coordinates; this reduced set is called a base. Our primary objective is the accurate determination of the energetics, i.e. heat release and temperature evolution. In Section I, we define the constituent radicals and describe the formation of the constituent radical base. In Section II, the behavior of the base set is examined in the context of a detailed reaction model for heptane combustion as given by LLNL investigators.[1] Finally, Section III is devoted to a discussion on how to use curve fits developed in Section II that describe rate and species behavior and to a perspective on the further work required to complete a reduced model for heptane (and other alkane) combustion.

[*]Senior Engineer.
[†]Senior Research Scientist, AIAA Associate Fellow (corresponding author, josette.bellan@jpl.nasa.gov).

I. Representation of species through a reduced base set

A. Heavy species decomposition into constituent radicals

Aside from the molar reaction rates, determining the temperature evolution in a reactive system requires knowledge of the species molar enthalpies and heat capacities. For species i, the molar enthalpy may be expressed as

$$h_i = h_i^0 + \widetilde{h}_i(T) \tag{1}$$

where h_i^0 is the heat of formation, $\widetilde{h}_i$ is the sensible enthalpy and T is the temperature. The heat of formation is taken at reference conditions, $p_{ref} = 1$ bar and $T_{ref} = 25$ C $= 298.15$ K where p is the pressure, giving

$$\widetilde{h}_i = \int_{T_{ref}}^{T} C_{p,i} dT \tag{2}$$

where $C_{p,i}$ is the molar constant-pressure heat capacity. A heat of combustion for species i is given by

$$h_i^c = h_i^0 - \sum_j w_{ji} h_j^0 \tag{3}$$

where the index j denotes the species set of air (O_2,N_2) and final combustion products (H_2O,CO_2). Equation 3 is based on water remaining in vapor state and not condensing into liquid. Consider the count of atoms (H,C,O,N) in species i. Hypothetically, we can consider species i as being composed of the air and final combustion product species. By definition, w_{ji} is the number of species j in species i that produces the correct atom count. The molar densities of species in this set are

$$N_j = N_j^0 - \sum_{i \neq j} w_{ji} N_i \tag{4}$$

where N_j^0 is the effective total molar density of species j. The same exercise of atom counting and species representation by the j set can be performed for all species in the mixture to obtain N_j^0. That is, the atomic elements molar densities are represented by species j molar densities. Conservation of atoms in the reactions makes unnecessary utilizing rate expressions for reaction coordinates of air species and complete-combustion products, as a one-to-one map exists between these and the atom set.

Using information from the NIST Chemistry WebBook website,[2] CRC Handbook of Chemistry and Physics,[3] the GRI website[4] and the NASA Glenn website,[5] plots of h_i^c for alkanes and also for alkenes having the carbon double bond at the molecular chain end (i.e. vinyl radical) show a linear variation with n (not shown). Further, at a fixed value of T, the corresponding $C_{p,i}$ also vary linearly with n. Both h_i^c and $C_{p,i}$ linear variation with n is functionally very accurate. This implies that these thermodynamic properties may be considered as determined by given properties of constituent radicals CH_2, CH_3 and C_2H_3 that together form these hydrocarbons. That is, each heavy species is decomposed into constituent radicals which are here used as their building blocks. This decomposition is consistent with the group additivity concept of Benson[6] (see also Reid et al.[7]); however, here it is desired to have forms with greater simplicity in which only first order (compositional) effects are allowed. For hydrocarbon species with double bonds not at the chain end or for oxidized species, the simplicity of constituent radicals as a base no longer rigorously, but only approximately, holds. To calculate h_i^c once either breakup of a hydrocarbon into free radicals or oxidation reactions occur, the assumption is made that one can associate a fixed partial enthalpy with each constituent radical, independent of the species to which they may belong. The information from the cited references shows that although this assumption is not entirely correct (when subtracting contributions from CH_2, CH_3 and C_2H_3), the variation across species is not substantial; as a result, an average over species is here taken. The error in the resulting h_i^c is rather small (not shown); two-digit accuracy is typically reached (with best accuracy for the dominant species).

Plots of C_p/R_u versus $\log T$, where R_u is the universal gas constant, are also nearly linear for the constituent radicals, as shown in Fig. 1. Thus, for this base, the form

$$\delta C_p/R_u = a^h + b^h \ln(T/T_{ref}) \tag{5}$$

is assumed with a^h and b^h being constant. Properties of any constituent radical in a stable molecule having valence bonds satisfied are not the same as when the radical is in free form, i.e. with one or more available

bonds. In the same manner, properties of heavy radicals are different from the sum of their constituent radicals. For example, the difference in heat of formation between constituent and free radical is defined as

$$\delta h^f = h^0_{\text{free radical}} - \delta h^0 \tag{6}$$

where δh^0 is the constituent radical partial heat of formation. For the set of 13 constituent bases listed in Table 1, values of $\delta h^0, \delta h^c, \delta h^f$, a^h and b^h are given in that table. The heavy species that are free radicals also require δh^f and δC_p corrections (i.e. additional a^h and b^h constants) due to unsatisfied valence bonds. These corrections may be estimated using increments in hydrogen bond strengths given by Lay et al.[8] along with information from LLNL[1] to NASA Glenn.[5] As an example, let R denote a radical produced by hydrogen abstraction; RH is the parent and E_b is the bond energy. Then,

$$h^0(RH) + \mathrm{E}_b = h^0(R) + h^0(H). \tag{7}$$

Also,

$$h^0(RH) = \delta h^0(R) + \delta h^0(H) \tag{8}$$

giving

$$\delta h^f(R) = \mathrm{E}_b + \delta h^0(H) - h^0(H) \tag{9}$$

with $\delta h^0(H) \simeq (10 n_b - 33)$ kJ/mol where n_b is the number of valence bonds of C atoms attached to the C atom of abstraction (e.g. $n_b = 0$ for methane, $n_b = 3$ for alkynes). The rules that were devised to estimate δh^f and δC_p for heavy radicals are given in Table 2 along with necessary corrections for a few stable molecules.

B. Light species as part of the base

The light species are not subject to meaningful decomposition. Values of h^c from the literature, C_p's fitted according to eq. 5 and other properties of the light molecules and light free-form of the constituent radicals are given in Table 3.

C. Final base set

The reaction base set is composed of 13 constituent radicals (Table 1) and 26 light molecules or free radicals (Table 3). The entire base set may not be needed for a particular situation. Furthermore, the atomic balance eliminates the need to calculate 4 of the light species.

II. Base behavior in stirred reactor heptane combustion

The evolution of T and the molar densities N_i was determined in test cases by utilizing the Chemkin II software package along with species and rate data from the LLNL website.[1] This data encompasses 160 species interacting through 1540 reaction rates (770 forward and 770 corresponding backward). The base set excludes dicarbon and also the light species (from Table 3) C, C_2, N, NO and NO_2 as they are not necessary (e.g. if the focus were on soot or NO_x, some of these species would enter the base set). Calculations were performed at initial pressures p_0 from 1 to 60 bar. Most calculations were performed for a stoichiometric mixture; a smaller number of calculations were made for molar equivalence ratios ϕ of 0.5 and 2.0.

To test the compatibility of using the constituent properties for finding the T evolution, the energy equation

$$NC_p \frac{dT}{dt} = -\sum_i h_i R_i, \qquad R_i \equiv \left(\frac{dN_i}{dt}\right)_{reaction} \tag{10}$$

where $N = \sum_i N_i$ and $NC_p = \sum_i N_i C_{p,i}$, was solved twice and simultaneously with different enthalpy inputs. In both cases, R_i is determined from the full rate LLNL[1] model; C_p and h_i were in one case determined through the LLNL model (which contains the enthalpies) and in the other case through the simplified forms given in Tables 1 through 3. The deviations between the two T profiles values were typically no more than 0.3% of the LLNL value (not shown); this is considered good accuracy. Thus, the overall model accuracy is not dependent on the C_p and h_i two thermal property assignments (ours versus LLNL), and instead depends on the accuracy in the values of R_i.

Using index k to denote members of the constituent radical set, the total constituent molar density

$$N_c = \sum_k N_k, \tag{11}$$

and constituent mole fractions

$$X_k = N_k/N_c. \tag{12}$$

A reference density for nitrogen N_2 is found from the dry air value at p_{ref} and T_{ref}, giving N_{ref}= 31.5 mol/m^3. Using N_{ref}, a dimensionless N_2 molar density is defined as

$$N^* \equiv \ N_{N_2}/N_{ref} \tag{13}$$

which acts as a convenient surrogate variable for p as the N^* value is essentially rate invariant. That is, the partial pressure of N_2 is the overwhelming contribution to p. Basically, the ratio of N^* to p_0 is nearly constant. The net constituent rate K_c is defined by

$$\frac{dN_c}{dt} = -K_c N_c. \tag{14}$$

A dimensionless temperature is also defined

$$\theta \equiv \frac{T - T_{in}(N^*)}{T_s} \tag{15}$$

where qualitatively $T_{in}(N^*)$ is the temperature at which K_c has a value large enough to signify combustion initiation, i.e. positive dT/dt, and T_s is such that N_c decreases from its initial value by three orders of magnitude (delving into higher order of magnitude decrease runs the risk of encountering round-off and truncation errors) at $\theta = 0.64$, a value chosen so that all θ values remain below unity for all test case calculations. A plot of T versus θ for stoichiometric heptane combustion is shown in Fig. 2 where the spread of values for T_s (the slope) and T_{in} (the ordinate at the origin) are shown. The variation of T_{in} is weak. As N^* increases, the change in slope decreases. Showing the appropriateness of the scaling with θ rather than using T, the evolution of N_c scaled by $(p_0 \times \phi)$ for p_0 = 1 bar and 10 bar and ϕ = 0.5, 1.0 and 2.0 is illustrated in in Fig. 3. Following the rule for finding T_s stated above, for ϕ = 0.5 and 2.0 its value is a factor of 0.67 and 1.17, respectively, that of T_s at $\phi = 1.0$. The normalization attainable with scaling is clear. Although it would be tempting to curve fit dN_c/dt from Fig. 3 and adopt it as a representative kinetic rate, the fact is that the scaling hides the precise detailed formulation that is required for a sufficiently accurate kinetics to predict T.

For stoichiometric combustion, a plot of $K_c(\theta, N^*)$ is depicted in Fig. 4. Quantitatively, the value of T_{in} corresponds to a value of K_c that is 2% of the minor first peak in K_c, with $T_{in} = O(800$ K). The value of K_c in Fig. 4 represents in fact only the small difference between the much larger production and loss rates which are nearly equal (not shown). This rate difference is about 1.5% to 2% of either production or loss rate at the minor peak, reaching a maximum at $\theta \approx 0.1$, just after the minima in K_c, then decreasing for $\theta \gtrsim 0.2$ to lows of O(0.1%) of the nearly equal production or loss rates. The maximum difference between production and loss rates is about 5% for $N^* \lesssim 1$, then decreases to about 3% at larger N^*. These maximum differences tend to occur during very large values of dT/dt. The small difference between production and loss is accurately captured, as the error tolerance in time marching is 10^{-9}, resulting in approximately a 7 place number accuracy. The relatively small difference between N_c production and loss suggests that K_c could be treated as a rate of a nearly quasi-steady process. Additionally, the region $\theta \lesssim 0.15$ is where T changes are relatively slow except near $\theta = 0.15$, but the degree of quasi-steadiness based on the production/loss rate differences is also lowest. The $\theta \lesssim 0.15$ range is a combustion incubation region, with reaction times values in ms units. The $\theta \gtrsim 0.2$ range is the fast reaction region with reaction times values in μs units. Curve fits to K_c in the two regions are plotted in Fig. 5. Shown on each Fig. 5a and Fig. 5b are 5 decades of kinetic rates and the agreement on the logarithmic scale is very good. Each test calculation, i.e. given N^*, is represented in Fig. 5 by a symbol type; the symbol location represents a selected sample of time stations during the calculation. The curve fits are based on all time stations at fixed intervals of $\Delta\theta$. The first interval is used for $\theta \lesssim 0.06$ and is small ($\simeq 10^{-3}$); the second interval is 5 times larger and is used for the remaining θ values.

Mean heat capacities and enthalpies, calculated as averages over the heavy (i.e. decomposed) species using the full rate (i.e. LLNL) model for N_i and R_i along with Tables 1 through 3 values, are defined as

$$C_{pm} = \sum_{i \subset (\text{heavy species})} \frac{C_{p,i} N_i}{N_c}, \qquad H_m = \sum_{i \subset (\text{heavy species})} \frac{h_i R_i}{K_c N_c}. \tag{16}$$

Plots of these means are presented in Fig. 6. Clearly, the extrema in H_m as function of θ occur at locations that are nearly independent of N^*; this behavior does not occur when scaling by T rather than θ. In particular, H_m is only weakly dependent on p_0 (i.e. N^*), featuring an apparent near singularity as $\theta \to 0$. The steep gradients in H_m and K_c near $\theta = 0$ indicate that, because these H_m and K_c values are multiplied in the energy equation, considerable care must be devoted to accurate modeling of the source terms in this incubation region. The 'noise' in Fig. 6a for $\theta > 0.6$ is due to numerical artifacts as $N_c \to 0$. The variation of C_{pm} shown in Fig. 6b is rather modest, which means that steep H_m gradients are due to the heat of combustion rather than to the sensible enthalpy contribution. This observation focusses the models on the R_k value and evolution, rather than on the direct T contribution to the H_m value.

So far, it is the kinetic rate of all the constituents, K_c that was fitted (Figs. 5a and 5b). The interest is now in examining the mole fraction of the constituents, X_k, to determine their behavior. If the situation were an equilibrium, then X_k would only depend on (N^*, θ, ϕ). Since the quasi-steadiness of N_c evokes small departures from equilibrium, it is natural to consider their timewise evolution through changes versus θ; thus X_k become functionals of θ and N^* at fixed ϕ. For stoichiometric combustion, plots of 8 dominant X_k are presented in Fig. 7. The evolution of these constituents was obtained with the full (i.e. LLNL) kinetics (implicitly including thermal properties) and serves to indicate what are the necessary attributes of the reduced model. The dependency on N^* is only pronounced as $N_c \to 0$, i.e. for large θ. The constituent radicals HOO, OO and C_2H_2 reach peak X_k values of $O(10^{-2})$ in the incubation region, then rapidly decrease. The peak occurs at $\theta \approx 0.025$ for the first two radicals, and at $\theta \approx 0.1$ for the last radical. Similar to Fig. 6, extrema tend to occur at fixed θ values confirming again the appropriateness of the T scaling to θ. For further modeling purposes, it may be noted that the partial heats of formation for HOO, OO and O stated in Table 1 depend on n_a, the number of carbon atoms in the radicals that are attached to the particular constituent radical. Because the variation of δh^0 with species identity for those particular constituents, average values are needed to calculate the T variation from the energy equation. The average values calculated using the LLNL model are -113 kJ/mol for HOO and O, and -42kJ/mol for OO.

Aside from air and combustion products, the light species CO, H_2, CH_4, H_2O_2, CH_2O, C_2H_4 and C_2H_2 have the largest molar density value of the light species in the base. The CO molar density dominates that of each of the other species in the list.

III. Summary and Conclusions

The species entering oxidation kinetics were categorized into either heavy or light species. For heavy species (i.e. those with carbon number ≥ 3), a constituent radical decomposition has been proposed. The constituent radicals and the light species form a base of small dimension used to follow the kinetics. It has been shown that modeled simplified expressions for constituent enthalpies lead to an adequately modeled heat release for heptane combustion. A simplified, low-dimensional chemistry model thus depends on an adequate representation of a reduced rate set, R_k, of the constituents. The net constituent rate, K_c, is nearly quasi-steady and may be split into an incubation region of modest temperature rise followed by a fast reaction region of high temperature. A degree of normalization of molar density behavior is achieved using scaled pressure and temperature variables, N^* and θ, respectively.

The incubation (small θ) region is characterized by roughly ms reaction times. These times are similar to diffusion time scales, and thus these processes are expected to significantly couple with the chemistry during incubation. When reducing the species to constituents, heavy species diffusion must be represented in this new framework. The question is then: What are appropriate diffusion coefficients? Since a particular constituent spans the entire heavy species set, a heavy species mean diffusion coefficient is appropriate. This means that heavy species differential diffusion cannot be considered in the incubation region. This is a problem encountered in any reduction scheme that focusses on modeling both the fully developed flame and the incubation region with the same reduced rate set. On the other hand, hypothetically, if a species is crucially affecting the incubation kinetics through differential diffusion, it can be selected to be part of the reduced set. Generally, using a reduced model in the incubation region, means that accuracy in this initial

evolution path is expected to be somewhat limited. This has implications for predicting ignition delay times.

In contrast to the incubation region, in the fast reaction zone the coupling between chemistry and flow processes is weak and combustion is primarily determined by the mixing rate. The behavior in the test cases using the LLNL species and rate data is that of very rapid temperature rise beginning at $\theta \approx 0.1$, i.e. at the transition of the incubation region to that of fast rate reactions. The temperature profiles in the fast rate region tend to be independent of the details of behavior during incubation, that is, an approach to a high-temperature 'attractor state' seems to prevail. Fortunately, this implies that any inaccuracies developed during incubation will be eventually eliminated. However, as mentioned above, special accuracy in modeling of the incubation region is needed.

Model closure will require the determination of effective mean source strengths for the light species and light radicals resulting from the heavy species. The final model will thus focus on reactions of the light species; the necessary rates are expected to be well determined insofar as kinetic interactions among light species prevail.

The constraint of atomic conservation enables a reduction in the number of rate progress variables by the number of atoms in the system. Formally, this could be applied to air and combustion products. However, from the viewpoint of numerical accuracy, these constraints are best applied to species (other than N_2), or species combinations, of relatively small mole fraction in order to minimize effects of round-off errors.

Acknowledgements

This work was conducted at the Jet Propulsion Laboratory (JPL), California Institute of Technology (Caltech) and sponsored by the Army Research Office under the direction of Drs. David Mann, Kevin McNesby and Ralph Anthenien.

References

[1]Lawrence Livermore National Laboratory website, http://www-cms.llnl.gov/combustion/combustion2.html

[2]National Institute of Standards and Technology, Chemistry WebBook website; http://webbook.nist.gov/chemistry/

[3]CRC Handbook of Chemistry and Physics, 86th Ed., D. R. Lide, Ed.-in-chief, CRC Press, Boca Raton, Fl., 2005 (internet edition)

[4]Gas Research Institute website, http://www.me.berkeley.edu/gri-mech/

[5]NASA Glenn Research Center website, http://cea.grc.nasa.gov/

[6]Benson, S. W., Thermochemical Kinetics., John Wiley & Sons, Inc., 1968

[7]Reid, R. C., Prausnitz, J. M. and Poling, B. E., The Properties of Gases and Liquids, McGraw-Hill Book Co., 4th edition, 1987, Chapt. 6

[8]Lay, T. H., Bozzelli, J. W., Dean, A. M. and Ritter, E. R., J. Chem. Phys., 99, 14514-14527, 1995

Radical	δh^0	δh^c	δh^f	a^h	b^h
CH_3 (methyl)	-42.0	714	188	3.137	3.433
CH_2 (methylene)	-20.8	614.3	411	2.784	2.812
CH (methylidyne)	$\cong$ -7	$\cong$ 507	$\cong$ 603	2.068	3.038
C_2H_3 (vinyl)	62.5	1212	237	4.432	4.468
C_2H_2 (CH=CH)$^{\otimes}$	73 $\pm$ 2	1102 $\pm$ 2	not relevant	3.82	3.72
C_2 (C$\equiv$C, dicarbon)	230	1017	608	2.919	1.796
HC_2 (HC$\equiv$C, ethynyl)	227	1135	339**	3.937	2.2515
CO (keto)	-133 $\pm$ 2	260.5	23	2.892	1.531
HCO (formyl)	-124 $\pm$ 3	390.3	167	3.5	2.1
HO (hydroxyl)	-166 $\pm$ 6***	-45	204	2.084	1.0945
HOO (hydroperoxy)$^{*\oplus}$	-205+116/n_a	-84+116/n_a	215-116/n_a	4.194	1.908
OO (peroxy)*	-16-13n_a	-16-13n_a	not relevant	3.65	2.135
O (ethers)$^{*\#}$	-74-13n_a	-74-13n_a	323+13n_a	-1.46	2.44

$^{\otimes}$trans: -2, cis: +2; for a molecule with one or more vinyl also present (i.e., polyene), $\delta C_p/R_u$ is increased by 12%;

**Alternate value (op. cit. NIST) is 250 from older data;

***value $\cong$ -180 if combined with CH radical;

$^{*}n_a$ is the number of carbon atoms in attached radicals;

$^{\oplus}$effective $n_a = 1.16$ with ring or branched attached radical;

$^{\#}$each of the two attachment points has a contribution to n_a, Δn_a, which has a maximum value of 2. The effective $n_a = 3$ for a ring with $n_a \geq 4$. If at least one vinyl is also present, then add the increment $\Delta n_a = +1$. For a ring with $n_a = 2$ or 3, a correction of 90 must be added to the δh^0 value listed in the table. $\delta C_p/R_u$ fit is for ring ethers; for a chain, $\delta C_p/R_u \cong 2.5$.

Note: if the keto (or formyl) radical is attached to oxygen (or hydroxyl), then a correction of -90 must be added to the δh^0 value listed in the table.

Table 1. Thermodynamic properties of constituent radicals. δh^0, δh^c, δh^f heats of formation, combustion, and component-to-free transition, respectively, in kJ/mol; constants a^h and b^h for partial molar heat capacity in the form $\delta C_p/R_u = a^h + b^h ln(T/T_{ref})$; T_{ref} = 25 C = 298.15 K.

Radical	δh^f (kJ/mol)	a^h	b^h
alkyl	182 (174)*	0.6	-1.5
alkenyl	235 (128)*	0.0	0.0
alkynyl	240 (133)*	1.2	-1.5
Q + OOH**	239	0.6	-2.8
alkyl +OO**	78	-0.7	-1.4
alkyl + O	147#	-1.3	0.5
alkyl + CO	160#	0.2	-0.6
Q + OO + OOH	140 (70)*	1.3	-3.8
Ring + O	226	3	-4
dienes (e.g. C_4H_5)	196 (90)*	0.0	0.0
Stable species	δh^c (kJ/mol)	a^h	b^h
Ring ether	90 (80 with 2 CH)	2.2	-2.5
nc[n]ket	not relevant	1.3	-1.8

*value with CH constituent or single bond C;
**for $n_a \leqslant 3$; if OOH is on a branch, use alkyl values;
#with alkenyl, subtract 20.

Table 2. Rules for enthalpy corrections for free radicals and enthalpy corrections for a few stable heavy molecules. $\delta C_p/R_u = a^h + b^h ln(T/T_{ref})$ for heavy free radicals and also corrections for ring ethers and ketohydroperoxy's (only nc[n]ket, where n is the carbon count in the species).

Molecule/Radical	h^0	h^c	a^h	b^h
H_2	0.0	241.5	3.282	0.400
O_2	0.0	0.0	3.476	0.5663
N_2	0.0	0.0	3.388	0.469
C	717	1111	2.50	0.0
H_2O	-241.5	0.0	3.688	1.217
CO_2	-393.5	0.0	4.690	1.390
N	473	473	2.50	0.0
H	218.0	339	2.50	0.0
HO	38	159	3.385	0.3637
HOO	10.5	131	4.150	1.307
O	249.2	249.2	2.536	0.0
CO	-110.5	283	3.426	0.4749
HCO	43.1	558	4.154	1.2875
CH_4	-74.6	802	3.797	4.305
CH_3	146	902	4.440	2.249
CH_2	390	1025	3.973	1.3015
CH	596	1110	3.220	0.7136
C_2H_3	300	1449	5.1	3.5
HC_2	566	1474	4.434	1.404
C_2	838*	1625	4.58	0.0
NO	90.3	90.3	3.533	0.4508
NO_2	33.2	33.2	4.691	1.151
H_2O_2	-136	106	5.269	1.880
HCOH	-109	526.5	4.27	2.546
C_2H_2	228	1257	5.368	2.294
C_2H_4	52.5	1323	5.383	4.676

*Alternate value of 832 from the CRC tables.

Table 3. Thermodynamic properties of molecules and free radicals. h^0 and h^c (heats of formation and combustion, respectively), in kJ/mol; constants a^h and b^h for molar heat capacity in the form $C_p/R_u = a^h + b^h ln(T/T_{ref})$; T_{ref} = 25 C = 298.15 K.

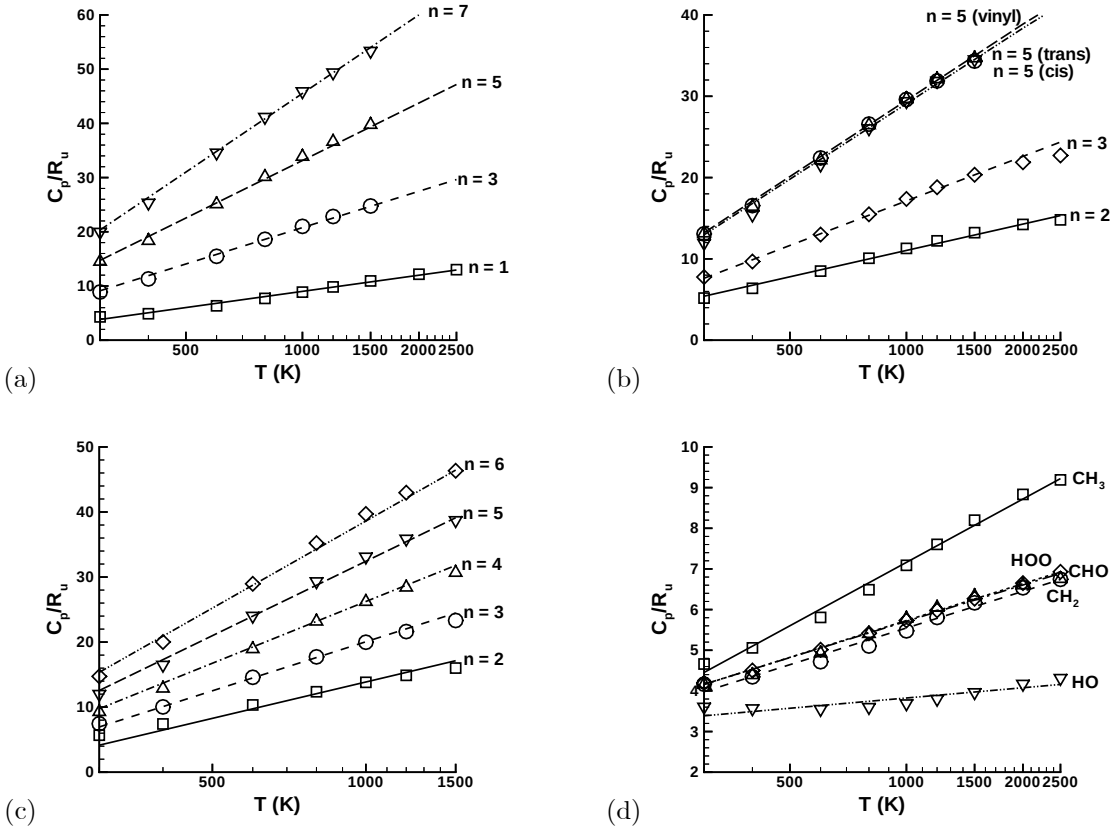

Figure 1. C_p/R_u **versus** $\log(T)$ **where** T **is in degrees K. Data values are in symbols; lines portray the fit constants. (a) alkanes (constants from Table 1); (b) alkenes (constants from Table 1); (c) ring ethers** $(CH_2)_nO$ **(constants from Table 1); and (d) some free radicals (constants from Table 3).**

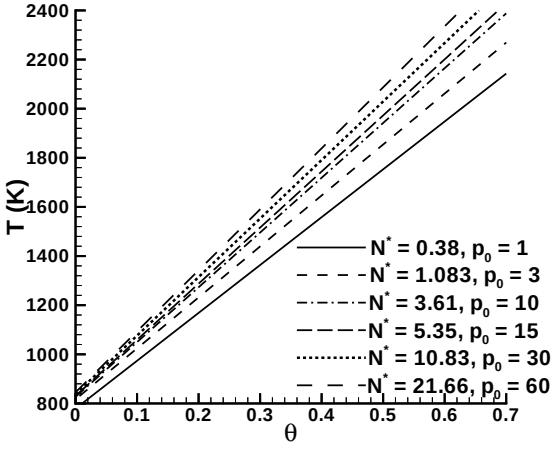

Figure 2. Temperature (in K) versus θ for various values of N^*. p_0 is in bar.

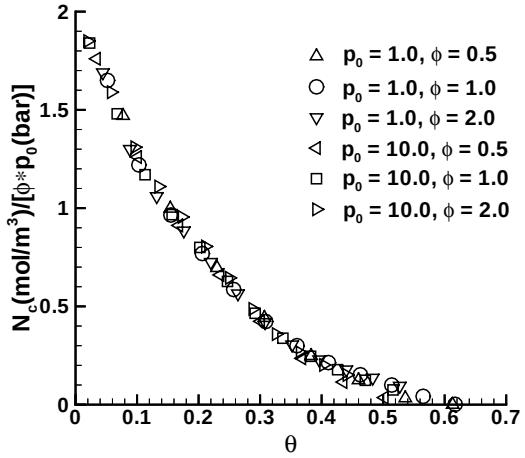

Figure 3. Evolution of the normalized N_c versus θ for $p_0 = 1$ bar and 10 bar for $\phi = 0.5$, 1.0 and 2.0.

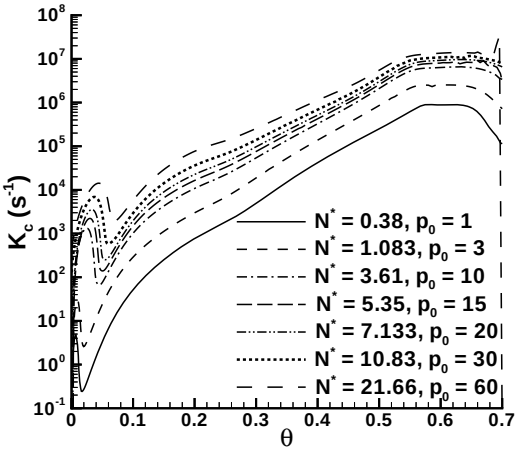

Figure 4. $K_c(\theta, N^*)$ **versus** θ **for stoichiometric combustion of heptane from test runs.** p_0 **is in bar.**

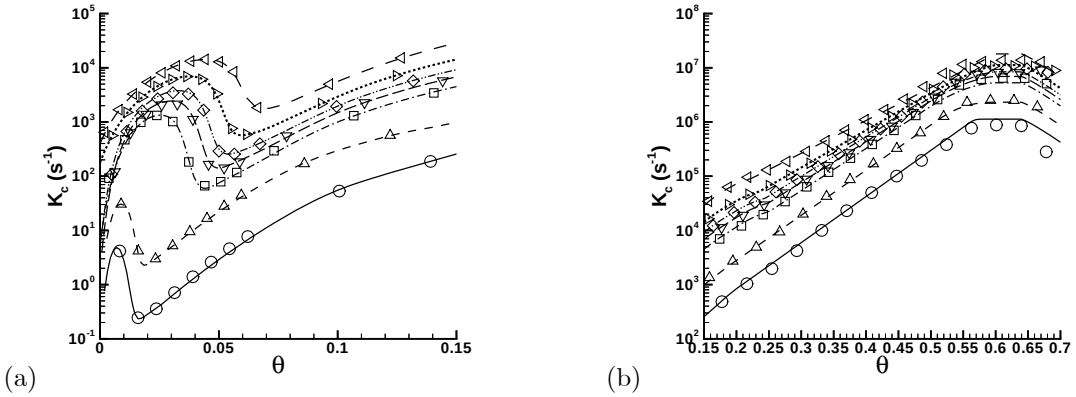

Figure 5. K_c **fits of the test runs in Fig. 4 for (a) the incubation region, and (b) the fast reaction region. Curves denote fits and the legend is the same as in Fig. 4; symbols denote selected full rate model values (the fits were based on all, i.e. not only the shown selected, values).**

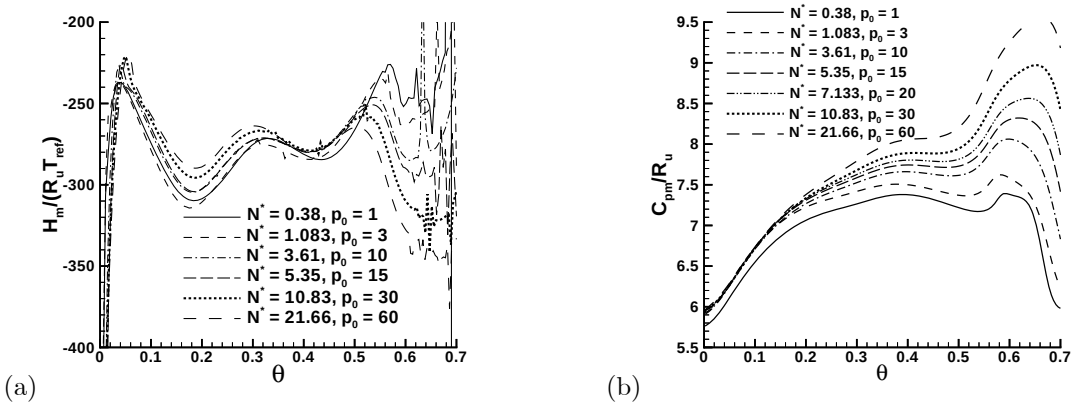

Figure 6. Mean values over the heavy species set as functions of θ **and** N^***. (a)** $H_m/(R_u T_{ref})$ **and (b)** C_{pm}/R_u**.** p_0 **is in bar.**

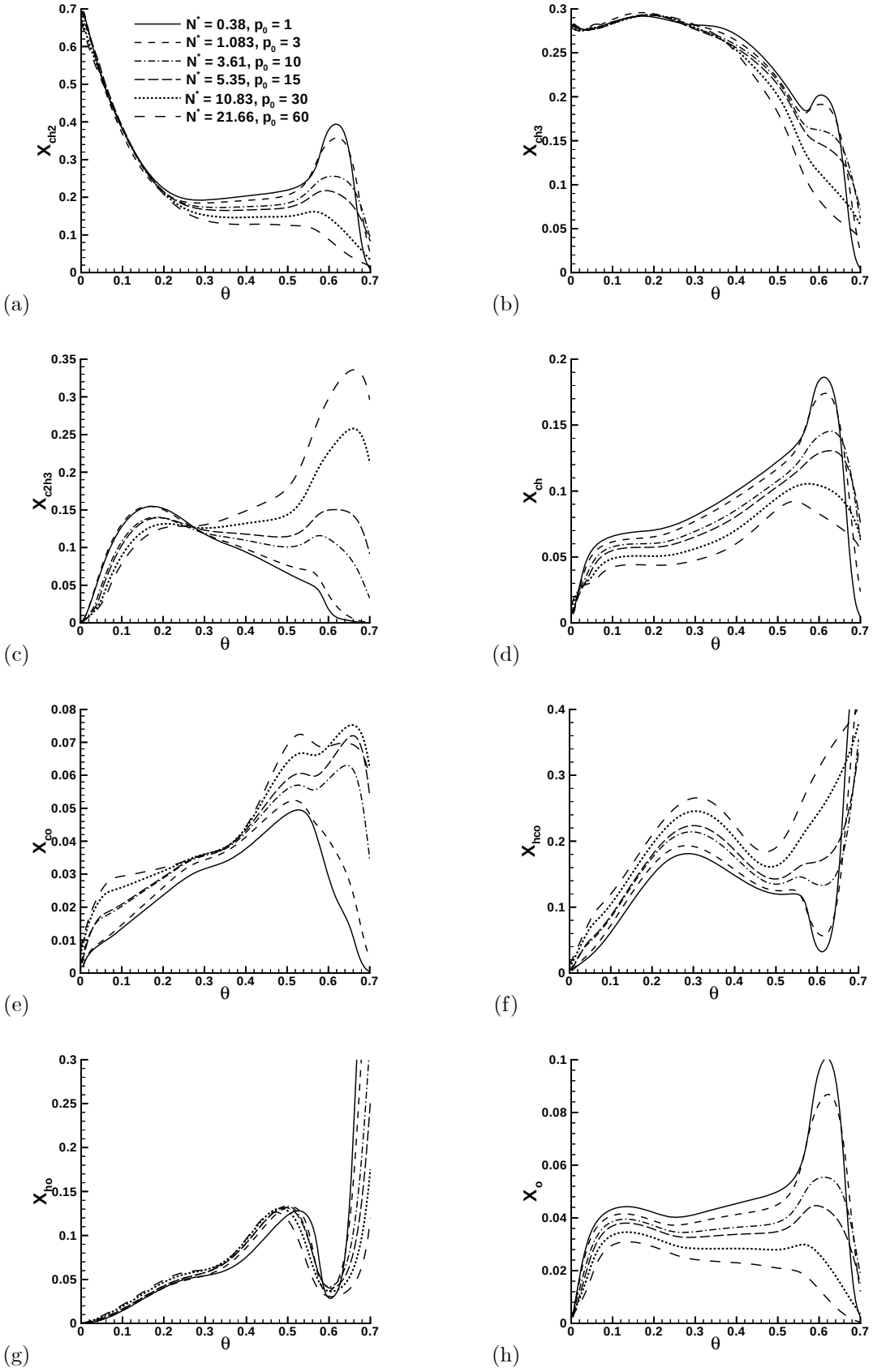

Figure 7. Constituent mole fractions X_k as functions of θ and N^* for $\phi = 1$. The constituent is (a) CH_2; (b) CH_3; (c) C_2H_3; (d) CH; (e) CO; (f) HCO; (g) HO; and (h) O. p_0 is in bar.

APPENDIX 2

A Simplified Model of Alkane Oxidation

Kenneth G. Harstad[♦,*] and Josette Bellan[♦,**,†]
Jet Propulsion Laboratory[♦], *California Institute of Technology,*
Pasadena CA 91109-8099
California Institute of Technology[**], *Mechanical Engineering, Pasadena, CA 91125*

A simplified model is proposed for the kinetics of alkane oxidation in air, based on a decomposition of heavy (carbon number greater or equal to 3) hydrocarbons into a 13 constituent radical base. The behavior of this base is examined in test computations for n-heptane utilizing Chemkin II with LLNL data inputs, placing emphasis on modeling to predict the heat release and temperature evolution. A normalized temperature was constructed which when used to plot the total constituent molar density divided by the product of the equivalence ratio and a nondimensional pressure, reveals a self-similar behavior of the plotted variable over a wide range of initial pressures and equivalence ratios. Examination of the LLNL kinetics shows that the total constituent molar density rate follows a quasi-steady behavior. This reaction rate was curve fitted along with the corresponding enthalpy production. The fits are shown against the normalized temperature for various equivalence ratios and initial nondimensional pressures and comparisons with the LLNL kinetics are very favorable. The model reduces the LLNL n-heptane mechanism from 160 species (progress variables) and 1540 reactions to 12 progress variables, 16 quasi-steady rates (associated with heavy species), 162 conventional reaction rates (light species) and 11 other functional forms (i.e. fits for the mean heavy-species heat capacity at constant pressure, the enthalpy release rate of the heavy species, and the molar fraction of quasi-steady light species). The proposed kinetic mechanism is valid over a pressure range from atmospheric to 60 bar, temperatures from 600 K to 2500 K and equivalence ratios from 0.125 to 8. This range encompasses diesel, HCCI and gas turbine engines, including cold ignition; and NO_x, CO and soot pollutant formation in the lean and rich regimes, respectively.

I. Introduction

Computational models for turbulent reactive flows present challenges that have yet to be fully met. First, combustion of typical hydrocarbons proceeds through the formation of hundreds of species interacting through thousands of reactions. Second, a complete numerical resolution of high Reynolds number flow requires a very large number of grid points that is beyond current typical supercomputer capabilities. Thus, combining detailed reaction rate models with the fundamental flow equations yields a numerical problem that is computationally prohibitive. A drastic (at least order of magnitude) reduction in the dimension of reaction kinetics is required for a feasible computational model. In spirit, this reduction is similar to that required in Large Eddy Simulations (where energetically significant flow scales are computed and the others are modeled) with respect to Direct Numerical Simulations (where all flow scales are computed). Since each species has a characteristic time scale, in the kinetic reduction it is also desirable to compute only those species having an essential characteristic time scale (to be defined) and model the kinetics of the remaining species.

We categorize all species involved in hydrocarbon oxidation into light species and heavy species; the heavy species are those having a carbon number $n \geqslant 3$. Based on this definition, a method for simplifying alkane combustion is proposed and tested for n-heptane. The method focusses on the total constituent radical molar density (see Section II definition and constituent radical base formation) of the heavy species rather than on the much larger number of these species. That is, rather than following all species through their reaction

*Senior Engineer.
†Senior Research Scientist, AIAA Fellow (corresponding author, josette.bellan@jpl.nasa.gov).

coordinates, we follow a reduced set of reaction coordinates; this reduced set is called a base. Our primary objective is the accurate determination of the energetics, i.e. heat release and temperature evolution; at this initial stage of model development, neither NO_x nor soot kinetics are addressed. In Section III, the behavior of the base set is examined in the context of a detailed reaction model for heptane combustion as given by LLNL[1] and the proposed model is tested against the LLNL kinetic scheme. Section IV is devoted to a discussion on the completion of the model. Finally, in Section V a summary of the accomplishments and a perspective on the future work are offered.

II. Species representation: a reduced base set

A. Heavy species decomposition into constituent radicals

Consider the count of atoms (H,C,O,N) in species i. We define w_{ji} as the number of species j in species i that produces the correct atom count, where the index j denotes the species set of air (O_2,N_2) and final combustion products (H_2O,CO_2). (This means that mathematically, we consider species i as being composed of air and final combustion product species.) The molar densities of species in this set are

$$N_j = N_j^0 - \sum_{i \neq j} w_{ji} N_i \tag{1}$$

where N_j^0 is the effective total molar density of species j. The same exercise of atom counting and species representation by the j set can be performed for all species in the mixture to obtain N_j^0. That is, the atomic elements molar densities are represented by species j molar densities. Conservation of atoms in the reactions makes unnecessary utilizing rate expressions for reaction coordinates of air species and complete-combustion products, as a one-to-one map exists between these and the atom set. The heavy species constituent radicals (CH_2, CH_3, CH, C_2H_3, C_2H_2, C_2, HC_2, CO (keto), HCO, HO, HO_2, OO, O) form a set of 13 entities from which any heavy species or radical may be constructed. The total constituent molar density is

$$N_c \equiv \sum_{k=1}^{13} N_k \tag{2}$$

where the molar density of constituent k is N_k. The decomposition into constituents is similar to group additivity,[2,3] except that it considers only first order (compositional) effects and only interactions with adjacent groups. The reaction rate associated with N_c is defined by

$$K_c \equiv -\frac{d(\ln N_c)}{dt}. \tag{3}$$

We define a reference density for nitrogen N_2 from the dry air value at pressure $p_{ref} = 1$ bar and T_{ref}= 298.15 K, giving N_{ref}= 31.5 mol/m^3. Using N_{ref}, a dimensionless N_2 molar density is defined as

$$N^* \equiv N_{N2}/N_{ref} \tag{4}$$

which acts as a convenient surrogate variable for the pressure p as the N^* value is essentially rate invariant. That is, the partial pressure of N_2 is the overwhelming contribution to p. Basically, the ratio of N^* to p_0 is nearly constant. A normalized temperature variable θ is defined by

$$\theta \equiv \frac{T - T_s}{T_r(\phi, N^*)}, \qquad T_r \equiv 2065(N^*)^{0.06} w(\phi), \qquad w(\phi) = \phi \frac{1.5 + 1.31\phi}{1 + 0.71\phi + 1.1\phi^2} \tag{5}$$

where T_s is a modeling parameter representing the lowest temperature at which $K_c > 0$. The θ definition is such that N_c decreases during stoichiometric combustion from its initial value by three orders of magnitude (delving into higher order of magnitude decrease runs the risk of encountering round-off and truncation errors) for $\theta \gtrsim 0.6$, a value chosen so that all θ values remain below unity for all test case calculations.

The contribution of the heavy group to the rate of change of a light species molar density N_i with mole fraction X_i (relative to the light group) is expressed in terms of quasi-steady gain and loss rates KG_i and KL_i as

$$\left.\frac{dN_i}{dt}\right|_{heavies} = N_c(KG_i - X_i KL_i). \tag{6}$$

Aside from the molar reaction rates, determining the temperature evolution in a reactive system requires knowledge of the species molar enthalpies and heat capacities. For species i, the molar enthalpy may be expressed as $h_i = h_i^0 + \widetilde{h}_i(T)$ where h_i^0 is the heat of formation, $\widetilde{h}_i$ is the sensible enthalpy and T is the temperature. The heat of formation is taken at the above reference conditions, giving $\widetilde{h}_i = \int_{T_{ref}}^{T} C_{p,i} dT$ where $C_{p,i}$ is the molar constant-pressure heat capacity. A heat of combustion for species i is given by

$$h_i^c = h_i^0 - \sum_j w_{ji} h_j^0 \tag{7}$$

under the assumption that water remains in vapor state. The energy equation is

$$\left(N_c C_{p,h} + \sum_{i \in lights} C_{p,i} N_i \right) \frac{dT}{dt} = - \sum_{i \in lights} h_i \mathcal{R}_i + N_c (R_u T_{ref}) K_h \tag{8}$$

where

$$\mathcal{R}_i \equiv (dN_i/dt)_{reac}, \tag{9}$$

R_u is the universal gas constant,

$$C_{p,h} \equiv (\sum_{l \in heavies} C_{p,l} N_l)/N_c, \tag{10}$$

and the rate of enthalpy change due to heavy species l chemical kinetic changes is defined as

$$K_h \equiv - \left(\sum_{l \in heavies} h_l \mathcal{R}_l \right) \frac{1}{R_u T_{ref} N_c}. \tag{11}$$

B. Light species as part of the base

Light species are not subject to meaningful decomposition according to the above procedure. Examination of runs made using the LLNL database indicate that the light species should be categorized in two subsets. The species in the first subset require rate equations and are part of the base set. The species in the second subset have a quasi-steady behavior and require fits of their mole fraction value as a function of the state variables (T, N^*, ϕ) and modeling parameters (here, only T_s). This first subset consists of: H_2O, CO_2, O_2, H, CO, H_2, CH_4, H_2O_2, C_2H_2, C_2H_4, CH_2O. The second subset are the radicals: O, CH, CH_2, CH_3, HO, HCO, HO_2, HC_2, C_2H_3. Thus this entire set consists of 20 light species. For their energetics, values of h^c are fitted from the literature and C_p's are obtained as

$$C_p/R_u = a^h + b^h \ln(T/T_{ref}). \tag{12}$$

Other properties of the light molecules and light free-form of the constituent radicals are given in Table 1.[4–7]

C. Final base set

The reaction base set is composed of a global (i.e. total) constituent radical and 11 light molecules or free radicals of the first subset (Table 1). Thus, there are only 12 progress variables. To compute N_c one must model K_c; to compute the 11 light species, one must model the KG_i, the KL_i, the X_i of the second subset and the conventional light species reaction rates of the first subset.

III. Results

A. Identification of a self-similar behavior

Showing the appropriateness of the scaling with θ rather than using T, the evolution of N_c scaled by $(\phi \times N^*)$ for fixed p_0 at several ϕ values and at fixed ϕ for several p_0 values is illustrated in Fig. 1 using the LLNL kinetics. The normalization attainable with θ scaling is clear and so is the fact that $N_c/(\phi \times N^*)$ is a similarity variable. At fixed $p_0 = 20$ bar, Fig. 1a, all $N_c/(\phi \times N^*)$ curves coincide nearly on the same curve, with the somewhat dissenting curve for $\phi = 4$ showing that for very rich mixtures there are indeed

constituents left after the oxidizer was depleted. However, even for as rich a mixture as $\phi = 2$, similarity holds, making this model valid in realms beyond those in advanced reduced schemes[8] where the upper limit of the scheme validity is $\phi = 1.5$, at most[9] $\phi = 2.0$ or exceptionally[10] $\phi = 3$. The behavior in Fig. 1a is typical of all fixed p_0 plots. In Fig. 1b, corresponding plots at stoichiometric conditions are shown, which are generic of all fixed ϕ plots. Again, the similarity achieved with the two normalized variables is remarkable, and only at a combination of high p_0 values and small T_s values (typical of the lowest T limit at which K_c rates are finite), are small to moderate departures from the excellent normalization perceptible.

We note that by $\theta \simeq [0.55, 0.6]$, $N_c \simeq 0$, meaning that modeling errors past that θ range are somewhat irrelevant to the model's accuracy since the reaction is practically finished. Although it would be tempting to curve fit dN_c/dt from Fig. 1 and adopt it as a representative kinetic rate, the fact is that the scaling hides the precise detailed formulation that is required for a sufficiently accurate kinetics to predict T. Thus, fits for K_c are instead needed to achieve appropriate accuracy, as discussed below.

Mo/Ra	h^0	h^c	a^h	b^h
H_2	0.0	241.5	3.282	0.400
O_2	0.0	0.0	3.476	0.5663
N_2	0.0	0.0	3.388	0.469
C	717	1111	2.50	0.0
H_2O	-241.5	0.0	3.688	1.217
CO_2	-393.5	0.0	4.690	1.390
N	473	473	2.50	0.0
H	218.0	339	2.50	0.0
HO	38	159	3.385	0.3637
HOO	10.5	131	4.150	1.307
O	249.2	249.2	2.536	0.0
CO	-110.5	283	3.426	0.4749
HCO	43.1	558	4.154	1.2875
CH_4	-74.6	802	3.797	4.305
CH_3	146	902	4.440	2.249
CH_2	390	1025	3.973	1.3015
CH	596	1110	3.220	0.7136
C_2H_3	300	1449	5.1	3.5
HC_2	566	1474	4.434	1.404
C_2	838*	1625	4.58	0.0
NO	90.3	90.3	3.533	0.4508
NO_2	33.2	33.2	4.691	1.151
H_2O_2	-136	106	5.269	1.880
HCOH	-109	526.5	4.27	2.546
C_2H_2	228	1257	5.368	2.294
C_2H_4	52.5	1323	5.383	4.676

*Alternate value of 832 from the CRC tables.

Table 1. Thermodynamic properties of molecules and free radicals. h^0 and h^c (heats of formation and combustion, respectively), in kJ/mol; constants a^h and b^h for molar heat capacity in the form $C_p/R_u = a^h + b^h ln(T/T_{ref})$; T_{ref} = 298.15 K. "Mo" denotes "molecule". "Ra" denotes "radical".

B. Global constituent molar density model

Plots of K_c versus θ show that there are two different regions of the curve. For small θ values, there is a combustion incubation region, with reaction times values in ms units. As θ increases, one encounters the fast reaction region with reaction times values in μs units. Numerous tests made with the LLNL kinetics showed that K_c represents only a small difference between production and loss rates which are nearly equal (not shown) and are much larger than K_c. The K_c value is typically about 1.5% to 5% of either production or loss rate. The maximum difference between production and loss rates is about 5% for $N^* \lesssim 1$, then decreases to about 3% at larger N^*. These maximum differences tend to occur during very large values of dT/dt. This fact suggests that K_c could be treated as a rate of a nearly quasi-steady process. If fits of K_c can be obtained over a significant region of parametric behavior, this model would be compact and represent a considerable reduction in the problem dimensionality. Noteworthy, had the approach been to find K_c from slopes of N_c in Fig. 1, it is clear that the important incubation region would have been missed.

Fitting K_c as a function of T and parameters N^*, ϕ and T_s presented a major challenge because of the non-monotonic K_c behavior and also because K_c spans so many decades. Fits were obtained by first inspecting the LLNL kinetics to understand the rate constant, K, variation. This variation showed an incubation region ($\theta \leq 0.2$) featuring first a maximum, K_{mx}, followed by a minimum, K_{mn}, and a high-T region ($\theta > 0.2$) where K_c monotonically increases. Thus, the functional fits are performed in three separate regions, with connection constraints between consecutive regions (the ultimate fits are piecewise continuous). The non-monotonic incubation-region behavior is captured by using a cubic functional mapping from $K(T)$ to $y(T)$ through the form

$$K(T) = \frac{1}{2}(K_{mx} + K_{mn}) + \frac{1}{4}(K_{mx} - K_{mn})(y^3 - 3y) \tag{13}$$

where $y(T) = -1$ at $T = T_{mx}$ which is the location of K_{mx} and $y(T) = 1$ at $T = T_{mn}$ which is the location of K_{mn}. In fact, the range of y is from slightly smaller than -2 at $T = T_s$ (i.e. $K_c > 0$) to $y \lesssim 1.8$. The values of K_{mx}, K_{mn}, T_{mx} and T_{mn} are fitted as polynomials in parameters $\ln(N^*), \ln(\phi)$ and $\ln(T_s/T_{ref})$. Also fitted is T_0 which is the T value at which $y = 0$. Two different changes of variables are made from $y(T)$ to $y(z)$ depending on how T compares to T_0. For $T < T_0$, a variable $z \equiv (T_0 - T)/(T_0 - T_{mx})$ is defined, which means that $y = -1$ at $z = 1$. To achieve the mapping, we first generate (y, z) pairs which are functions of parameters $\ln(N^*), \ln(\phi)$ and $\ln(T_s/T_{ref})$. To match these pairs, a ratio of appropriate functions (e.g. polynomials $a + bz + cz^2 + ...$; power functions of type a^z; and combinations of the two functional forms) is chosen to produce the $y(z)$ mapping. For $T > T_0$, i.e. $y \geqslant 0$, a similar procedure is used for $y(z)$ where now $z \equiv (T - T_0)/(T_{mn} - T_0)$. Beyond incubation, for the high-T region, $\ln(K)$ is fitted as a fifth order polynomial in θ^p where $p = 1$ for $\phi \leqslant 0.5$ and $p = (0.86 + 0.28\phi)/(0.74 + 0.52\phi)$ for $\phi > 0.5$. Scrutiny of the LLNL kinetics showed that the largest value of T_s is 825 K. Then, for $T_s = 825$ K, the polynomial coefficients were fitted, separately for the lean/stoichiometric ($\phi \leqslant 1$) and rich ($\phi > 1$) regions, as polynomials in $\ln(N^*)$ and $\ln(\phi)$. To obtain fits for $T_s < 825$ K, a scaling procedure was used from the $T_s = 825$ K fits to match particular K values at a specific point in the incubation region.

All fits further presented in Figs. 2-6 have been achieved with the fixed set of mapping functions described above. That is, no local corrections of any sort were used, nor exceptions from those functions were considered. Local corrections in a four-dimensional space are not computationally practical.

Curve fits to K_c computed using the LLNL kinetics are plotted in Figs. 2-4. In Fig. 2a and 2b (fixed p_0, various ϕ and T_s), and Fig. 3a and 3b (fixed ϕ in the lean regime, various p_0 and T_s) we differentiate between the incubation and fast-reaction regions discussed above and show on each figure up to 5 decades of kinetic rates. On each figure, symbols represent the LLNL-based computation and the symbol location represents a selected sample of time stations during the calculation. The curve fits are shown as lines and are based on time stations at fixed intervals of $\Delta\theta$. The agreement on the logarithmic scale is excellent to very good and deterioration of the fits at $\theta \gtrsim 0.55$ correspond to very small values of N_c, as noted above. Particularly important is the excellent agreement between fits and LLNL kinetics in the region of $\theta \leq 0.2$ representing 54% of the N_c decay (see Fig.1). For $\theta > 0.2$ the agreement is still excellent as long as T_s is not too low; good agreement still occurs in the significant N_c regions (i.e. $\theta \lesssim [0.55, 0.6]$) and over a much wider ϕ range than usually shown in the literature. Figure 4a focusses on the rich regime, showing the entire range of relevant θ (see Fig. 1a) at various p_0 and T_s. The agreement of fits with the LLNL data is excellent, bodying well for future studies addressing soot and CO formation. Noteworthy, the fits encompass a wide p_0 range including the desired high-pressure situations for engine combustion, and a much wider ϕ range than typically used in kinetic reduction schemes[8] where generally $\phi \in [0.5, 1.5]$, sometimes[9] $\phi \in [0.5, 2.0]$ and exceptionally[10] $\phi \in [0.7, 3.0]$. To show the influence of T_s, in Fig. 4b is depicted the case for which the widest range of T_s was available, corresponding to $p_0 = 10$ bar and $\phi = 1$. Similar to the other figures, the agreement with the LLNL kinetics is excellent to very good up to $\theta \leq 0.2$ and somewhat deteriorates past that station.

This deterioration is a manifestation of the need for matching two different functional forms: one in the incubation region ($y > 0$), and the other in the high-T region. The matching point is at $y_{\max}$; as $y_{\max}$ increases, the high-T region fit improves while the incubation fit worsens, and vice versa for decreasing $y_{\max}$. Fits can also be improved if one is less ambitious in covering the large ϕ range treated here. The functional behavior of ϕ outliers is somewhat different from that for moderate ϕ. For $\phi < 1$ and small, the high-T rates are quite modest and below K_{mx}. For $\phi > 1$, as ϕ increases, the ratio K_{mx}/K_{mn} decreases and high-T rates exceed K_{mx} except for the largest ϕ where the reaction terminates before the K_{mx} value is reached again in the high-T region. This behavior is independent of p_0. This is to say that if the ϕ outliers are eliminated, a much simpler picture arises and consequently more accurate fits are possible. Conceptually, one could also improve the fits by using a larger number of parameters in the model, however, this would defeat the purpose of computational efficiency that is the basis for seeking reduced kinetics.

C. Recovery of the energetics

According to eq. 8, to recover the value of T in the reduction scheme, the heavy species model should focus on an appropriate representation of $C_{p,h}$ and K_h. Plots (not shown) of $C_{p,h}$ at various p_0 values, calculated using the LLNL model over a wide range of ϕ, show that these curves exhibit a very modest variation over the range of strong N_c decay; moderate (i.e. up to 50%) variation occurs only after N_c values are very small to negligible. This indicates that the T recovery is primarily governed by K_h as far as heavy species

modeling is concerned.

Examples of K_h model fits to the LLNL calculated values are shown in Figs. 5 and 6. First, it is clear that the plots resemble functionally those of K_c, which is not surprising given the definitions of eqs. 3 and 11. Second, the energetics is remarkably well recovered for a variety of ϕ and T_s (Fig. 5), including very rich mixtures (Fig. 6). Similarly, excellent to very good results are obtained for lean mixtures (not shown). Should more accurate K_h fits be desirable, the K_c discussion on this topic is entirely pertinent.

IV. Completing the kinetic model

While a detailed discussion of the remaining kinetic-model parts is not presented, the process to complete the model is clear. The model is completed with the fitting of quasi-steady gain rates KG_i (where i stands for H_2O, CO_2, O_2, H, CO, H_2, CH_4, H_2O_2, C_2H_2, C_2H_4, CH_2O), of quasi-steady loss rate KL_i (where i stands for H_2O, O_2, H, H_2, this rate being null for the other light species) and of the quasi-steady light species mole fraction X_i. To show that the K_c fitting has set a methodology for completing the model, displayed in Fig. 7 is the quasi-steady rate function KG for CO at $p_0 = 30$ bar. The plot was obtained using the LLNL kinetics. Function KG_{CO} represents the net gain of molar density N_{CO} due to all rates involving the heavy species group (note: KL_{CO} is null). The plot graphically resembles K_c and K_h, indicating a consistent quasi-steady functional behavior for the heavy group contribution similar to that previously identified for K_c. Moreover, with increasing ϕ beyond $\phi = 1$, an asymptotic self-similar behavior is evident in the fast reaction regime. This plot is typical of all KG_i rates and shows that the same fitting methodology used for K_c and K_h will apply.

Regarding the rates KL_i (except for possibly i =H), they also have the specific graphical form (not shown) seen for K_c, K_h and KG_{CO}; thus, for constructing KL_i and X_i fits, the same basic fitting methodology will apply as for K_c and K_h.

V. Conclusions

The LLNL heptane kinetic model has been examined focussing on a potential very computationally efficient kinetic reduction scheme. Species were categorized into light or heavy (C number $n \geqslant 3$). The heavy species were decomposed into defined 13 constituents, and it was shown that a non-dimensional temperature θ depending on the pressure variable N^* and the equivalence ratio ϕ can be defined so that the ratio of the total constituent molar density N_c to the product of equivalence ratio and a nondimensional pressure N^* exhibits a self-similar behavior over a wide range of initial p_0, ϕ and a model-defined temperature T_s entering the computation of θ. The number of progress variables is thus reduced from 160 progress variables to 12 (11 for perfectly stirred reactor cases where H is also quasi-steady): the unsteady light species and N_c.

Assessment of the total constituent reaction rate, K_c, behavior revealed that it is quasi-steady and features two distinct regimes: incubation and fast reaction. The rate was fitted in terms of a total of four parameters: the physical parameters T or θ (a surrogate for T), ϕ, N^* and a modeling parameter T_s; θ itself is a function of ϕ, N^* and T_s. The same functions were used to achieve the fits over the entire region covered by the four parameters. These plots reproduced with excellent to very good accuracy the reaction rate over the significant lifetime of the total constituent and for a range of p_0 and ϕ that is much wider than the typical one used for displaying reduced mechanisms. The energetics associated with the heavy species reaction rate, K_h, was also recovered through fits which were functionally similar to those for K_c. Expectably, it is found that the K_h value rather than the value of the heavy species heat capacities at constant pressure, $C_{p,h}$, contributes mostly to the enthalpy change associated with the heavy species reaction. The $C_{p,h}$ also requires fitting. Mathematically, the shown fits achieved substantial accuracy over seven rate decades considering the fact that they depend upon four variables.

The model is completed once the gain/loss of light species molar density from the heavy species and the mole fraction X_i (relative to the light group) of quasi-steady light species are fitted. Examination of these gain/loss rates shows that they also have a quasi-steady behavior. As an example, it was shown that the gain-rate functional form with respect to θ emulates those of K_c and K_h, making the modeling strategy clear. This finding highlights the fact that the fitting technique provides a methodology which can be repeatedly used to obtain an accurate representation of full or skeletal kinetic models. The advantage of the proposed model is that the kinetic reduction is performed before embedding the kinetics in a turbulent flow computation and would be used as a library of rates rather than needing 'on-the-fly' kinetic rate calculations.

Summarizing, the proposed model features 12 ultimate progress variables describing heptane oxidation. The model requires fitting 16 quasi-steady rate functions, 11 curves for light quasi-steady mole fractions, and $C_{p,h}$. Also required are conventional rates between members of the light group, which are available in the literature. Because this model is based on the N_c rate rather than on that of individual heavy species, even if the number of species increases with increased C number in the alkane group, providing that the quasi-steady rate aspect persists, then extension of this model to higher alkanes should be conceptually straightforward; although it remains to be seen if the functional fits would remain valid or would require reconstruction.

Acknowledgements

This study was conducted at the Jet Propulsion Laboratory (JPL), California Institute of Technology (Caltech) and sponsored at Caltech by the Army Research Office under the direction of Drs. David Mann, Kevin McNesby and Ralph Anthenien.

References

[1]Lawrence Livermore National Laboratory,http://www-cms.llnl.gov/combustion/combustion2.html.

[2]S. W. Benson, Thermochemical Kinetics., John Wiley & Sons, Inc., 1968.

[3]R. C. Reid, J. M. Prausnitz, B. E. Poling, 1987 The Properties of Gases and Liquids, McGraw-Hill Book Co., 4th edition, Chapt. 6.

[4]National Institute of Standards and Technology, Chemistry WebBook; http://webbook.nist.gov/chemistry/.

[5]CRC Handbook of Chemistry and Physics, 86th Ed., D. R. Lide, Ed.-in-chief, CRC Press, Boca Raton, Fl., 2005 (internet edition).

[6]Gas Research Institute, http://www.me.berkeley.edu/gri-mech/.

[7]NASA Glenn Research Center, http://cea.grc.nasa.gov/.

[8]T. Lu, C. K. Law, 2006 Linear time reduction of large kinetic mechanisms with directed relation graph: n-heptane and iso-octane, *Combust. Flame,* 144, 24-36.

[9]N. Peters, G. Paczko, R. Seiser, K. Sheshadri, 2002 Temperature cross-over and non-thermal runaway at two-stage ignition of n-heptane, *Combust. Flame,* 128, 38-59.

[10]V. I. Babushok, W. Tsang, 2004 Kinetic modeling of heptane combustion and PAH formation, *J. Propul. Power*, 20(3), 403-414.

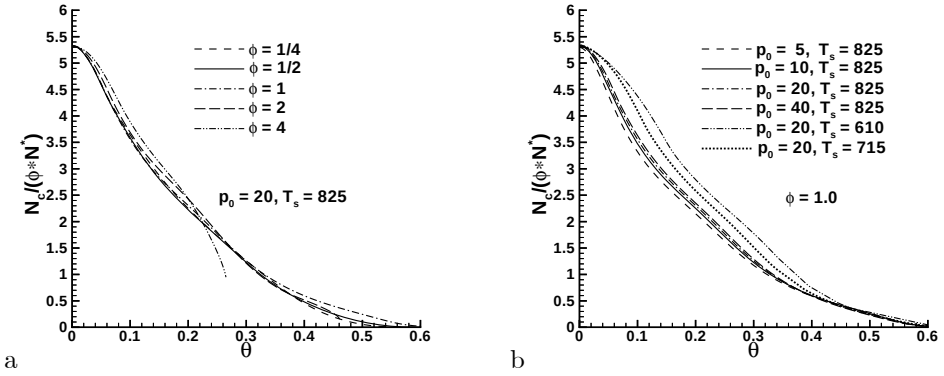

Figure 1. Similarity plots of parameter $N_c/(\phi \times N^*)$ versus θ at (a) $p_0 = 20$ bar and (b) $\phi = 1$. T_s is in K.

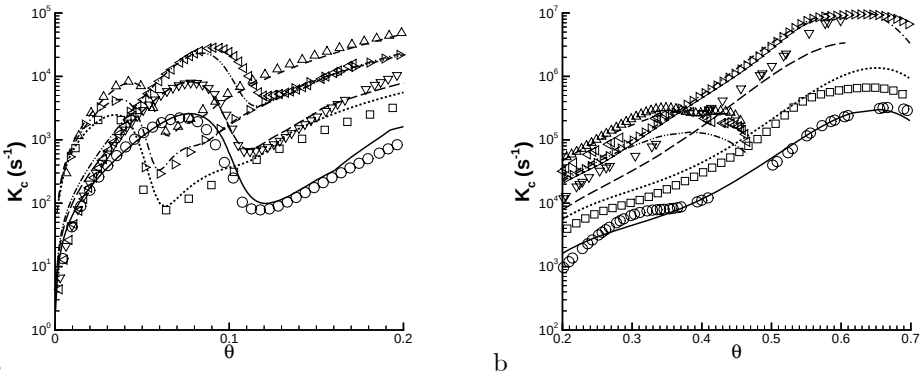

Figure 2. K_c **versus** θ **for** $p_0 = 20$ **bar. Symbols** $\square, \triangleright, \Delta, \bigcirc, \nabla, \triangleleft$ **represent selected data from the LLNL runs; lines** $\bullet\bullet\bullet, -\bullet-\bullet-$**,- - -,** ——**,** $---$**,** $-\bullet\bullet-\bullet\bullet-$ **represent the corresponding fits. Temperatures units are in degrees K. The legend is:** $\bullet\bullet\bullet$ $\phi = 0.5$, $T_s = 825$; —— $\phi = 0.5$, $T_s = 715$, $-\bullet-\bullet-$ $\phi = 1.0$, $T_s = 825$; $---$ $\phi = 1.0$, $T_s = 715$; - - - $\phi = 2.0$, $T_s = 825$; $-\bullet\bullet-\bullet\bullet-$ $\phi = 2.0$, $T_s = 715$.

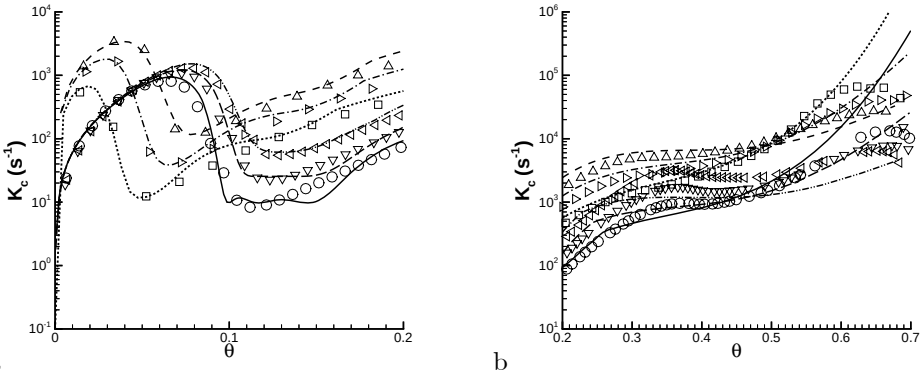

Figure 3. K_c **versus** θ **for** $\phi = 1/3$ **at different** p_0 **and** T_s**. Symbols** $\square, \triangleright, \Delta, \bigcirc, \nabla, \triangleleft$ **represent selected data from the LLNL runs; lines** $\bullet\bullet\bullet, -\bullet-\bullet-$**,- - -,** ——**,** $---$**,** $-\bullet\bullet-\bullet\bullet-$ **represent the corresponding fits. Units: pressures in bar, temperatures in degrees K. The legend is:** $\bullet\bullet\bullet$ $p_0 = 10$, $T_s = 825$; —— $p_0 = 10$, $T_s = 715$, $-\bullet-\bullet-$ $p_0 = 20$, $T_s = 825$; $---$ $p_0 = 20$, $T_s = 715$; - - - $p_0 = 40$, $T_s = 825$; $-\bullet\bullet-\bullet\bullet-$ $p_0 = 40$, $T_s = 715$.

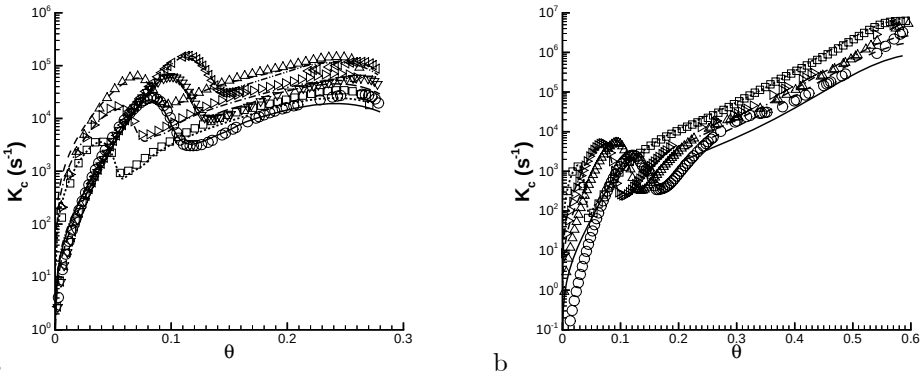

Figure 4. K_c **versus** θ **for a variety of conditions. Symbols** $\square, \triangleright, \Delta, \bigcirc, \nabla, \triangleleft$ **represent selected data from the LLNL runs; lines** $\bullet\bullet\bullet, -\bullet-\bullet-$**,- - -,** ——**,** $---$**,** $-\bullet\bullet-\bullet\bullet-$ **represent the corresponding fits. Units: pressures in bar, temperatures in degrees K. (a)** $\phi = 4$**, (**$\bullet\bullet\bullet$ $p_0 = 10$, $T_s = 825$; —— $p_0 = 10$, $T_s = 715$, $-\bullet-\bullet-$ $p_0 = 20$, $T_s = 825$; $---$ $p_0 = 20$, $T_s = 715$; - - - $p_0 = 40$, $T_s = 825$; $-\bullet\bullet-\bullet\bullet-$ $p_0 = 40$, $T_s = 715$**). (b)** $p_0 = 10$ **and** $\phi = 1$ **(**$\bullet\bullet\bullet$ $T_s = 825$; —— $T_s = 715$, $-\bullet-\bullet-$ $T_s = 655$; $---$ $T_s = 560$**).**

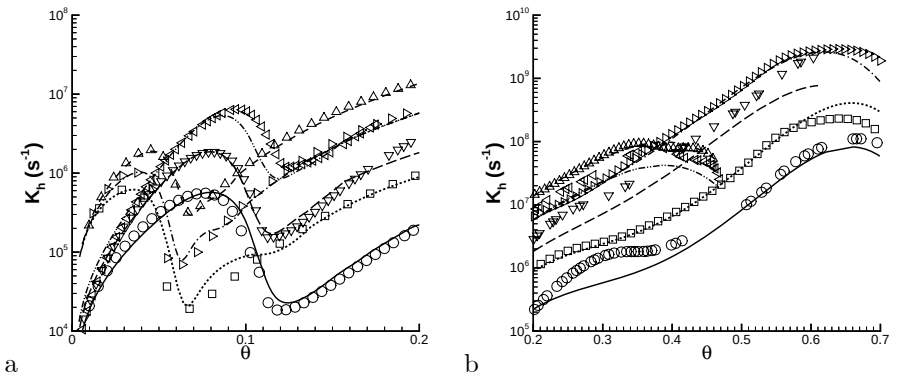

Figure 5. K_h **versus** θ **at fixed** $p_0 = 20$ **bar for different** ϕ **and** T_s **values corresponding to (a) Fig. 2a, and (b) Fig. 2b. The legend is in Fig. 2 caption.**

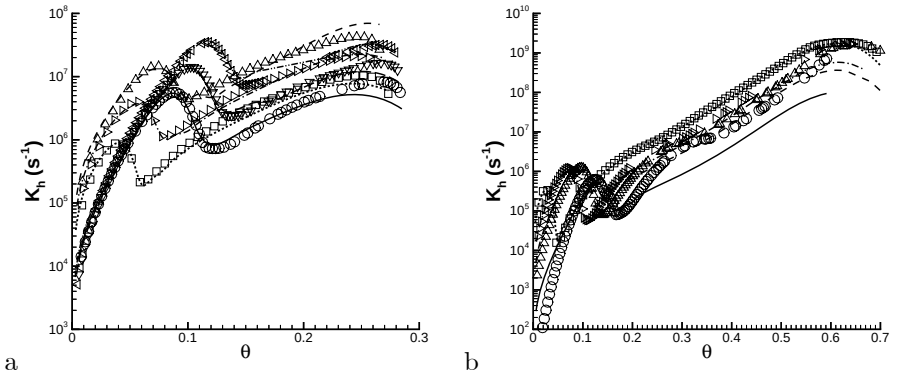

Figure 6. K_h **versus** θ **for (a)** $\phi = 4$ **corresponding to Fig. 4a, and (b)** $\phi = 1$ **and** $p_0 = 10$ **bar corresponding to Fig. 4b. The legend is in Fig. 4 caption.**

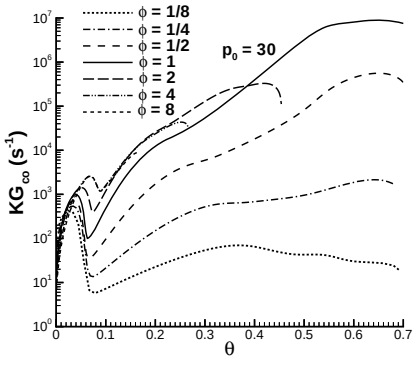

Figure 7. KG **for CO versus** θ**.** p_0 **is in bar. Plots obtained using the LLNL data in CHEMKIN II.**

APPENDIX 3

Computationally efficient modeling of n-heptane oxidation using constituents and species

K. G. Harstad[1] and J. Bellan[1,2]

[1] *Jet Propulsion Laboratory, California Institute of Technology*
[2] *California Institute of Technology, Mechanical Engineering Department*

Abstract

A simplified model is proposed for the kinetics of alkane oxidation in air, based on a decomposition of heavy (carbon number greater or equal to 3) hydrocarbons into a 13 constituent radical base. The behavior of this base is examined in test computations for n-heptane utilizing Chemkin II with LLNL data inputs, placing emphasis on modeling to predict the heat release and temperature evolution. A normalized temperature was constructed which when used to plot the total constituent molar density divided by the product of the equivalence ratio and a nondimensional pressure, reveals a self-similar behavior of the plotted variable over a wide range of initial pressures and equivalence ratios. Examination of the LLNL kinetics shows that the total constituent molar density rate follows a quasi-steady behavior. This reaction rate was curve fitted along with the corresponding enthalpy production. The fits are shown against the normalized temperature for various equivalence ratios and initial nondimensional pressures and comparisons with the LLNL kinetics are very favorable. The model reduces the LLNL n-heptane mechanism from 160 species (progress variables) and 1540 reactions to 12 progress variables, 16 quasi-steady rates (associated with heavy species), 162 conventional reaction rates (light species) and 11 other functional forms (i.e. fits for the mean heavy-species heat capacity at constant pressure, the enthalpy release rate of the heavy species, and the molar fraction of quasi-steady light species). The proposed kinetic mechanism is valid over a pressure range from atmospheric to 60 bar, temperatures from 600 K to 2500 K and equivalence ratios from 0.125 to 8. This range encompasses diesel, HCCI and gas turbine engines, including cold ignition; and NO_x, CO and soot pollutant formation in the lean and rich regimes, respectively.

Keywords: reduced n-heptane kinetics

1. Introduction

Computational models for turbulent reactive flows present challenges that have yet to be fully met. First, combustion of typical hydrocarbons proceeds through the formation of hundreds of species interacting through thousands of reactions. Second, a complete numerical resolution of high Reynolds number flow requires a very large number of grid points that is beyond current typical supercomputer capabilities. Thus, combining detailed reaction rate models with the fundamental flow equations yields a numerical

problem that is computationally prohibitive. A drastic (at least order of magnitude) reduction in the dimension of reaction kinetics is required for a feasible computational model. In spirit, this reduction is similar to that required in Large Eddy Simulations (where energetically significant flow scales are computed and the others are modeled) with respect to Direct Numerical Simulations (where all flow scales are computed). Since each species has a characteristic time scale, in the kinetic reduction it is also desirable to compute only those species having an essential characteristic time scale (to be defined) and model the kinetics of the remaining species.

We categorize all species involved in hydrocarbon oxidation into light species and heavy species; the heavy species are those having a carbon number $n \geqslant 3$. Based on this definition, a method for simplifying alkane combustion is proposed and tested for n-heptane. The method focusses on the total constituent radical molar density (see Section 2 definition and constituent radical base formation) of the heavy species rather than on the much larger number of these species. That is, rather than following all species through their reaction coordinates, we follow a reduced set of reaction coordinates; this reduced set is called a base. Our primary objective is the accurate determination of the energetics, i.e. heat release and temperature evolution; at this initial stage of model development, neither NO_x nor soot kinetics are addressed. In Section 3, the behavior of the base set is examined in the context of a detailed reaction model for heptane combustion as given by LLNL [1] and the proposed model is tested against the LLNL kinetic scheme. Section 4 is devoted to a discussion on the completion of the model. Finally, in Section 5 a summary of the accomplishments and a perspective on the future work are offered.

2. Species representation: a reduced base set

2.1. Heavy species decomposition into constituent radicals

Consider the count of atoms (H,C,O,N) in species i. We define w_{ji} as the number of species j in species i that produces the correct atom count, where the index j denotes the species set of air (O_2,N_2) and final combustion products (H_2O,CO_2). (This means that mathematically, we consider species i as being composed of air and final combustion product species.) The molar densities of species in this set are

$$N_j = N_j^0 - \sum_{i \neq j} w_{ji} N_i \tag{1}$$

where N_j^0 is the effective total molar density of species j. The same exercise of atom counting and species representation by the j set can be performed for all species in the mixture to obtain N_j^0. That is, the atomic elements molar densities are represented by species j molar densities. Conservation of atoms in the reactions makes unnecessary utilizing rate expressions for reaction coordinates of air species and complete-combustion products, as a one-to-one map exists between these and the atom set. The heavy species constituent radicals (CH_2, CH_3, CH, C_2H_3, C_2H_2, C_2, HC_2, CO (keto), HCO, HO, HO_2, OO, O) form a set of 13 entities from which any heavy species or radical may be constructed. The total constituent molar density is

$$N_c \equiv \sum_{k=1}^{13} N_k \tag{2}$$

where the molar density of constituent k is N_k. The decomposition into constituents is similar to group additivity [2, 3], except that it considers only first order (compositional) effects and only interactions with adjacent groups. The reaction rate associated with N_c is defined by

$$K_c \equiv -\frac{d(\ln N_c)}{dt}. \tag{3}$$

We define a reference density for nitrogen N_2 from the dry air value at pressure p_{ref} = 1 bar and T_{ref}= 298.15 K, giving N_{ref}= 31.5 mol/m^3. Using N_{ref}, a dimensionless N_2 molar density is defined as

$$N^* \equiv N_{N2}/N_{ref} \tag{4}$$

which acts as a convenient surrogate variable for the pressure p as the N^* value is essentially rate invariant. That is, the partial pressure of N_2 is the overwhelming contribution to p. Basically, the ratio of N^* to p_0 is nearly constant. A normalized temperature variable θ is defined by

$$\theta \equiv \frac{T - T_s}{T_r(\phi, N^*)} \tag{5}$$

$$T_r \equiv 2065 (N^*)^{0.06} w(\phi) \tag{6}$$

$$w(\phi) = \phi \frac{1.5 + 1.31\phi}{1 + 0.71\phi + 1.1\phi^2} \tag{7}$$

where T_s is a modeling parameter representing the lowest temperature at which $K_c > 0$. The θ definition is such that N_c decreases during stoichiometric combustion from its initial value by three orders of magnitude (delving into higher order of magnitude decrease runs the risk of encountering round-off and truncation errors) for $\theta \gtrsim 0.6$, a value chosen so that all θ values remain below unity for all test case calculations.

The contribution of the heavy group to the rate of change of a light species molar density N_i with mole fraction X_i (relative to the light group) is expressed in terms of quasi-steady gain and loss rates KG_i and KL_i as

$$\left.\frac{dN_i}{dt}\right|_{heavies} = N_c(KG_i - X_i KL_i). \tag{8}$$

Aside from the molar reaction rates, determining the temperature evolution in a reactive system requires knowledge of the species molar enthalpies and heat capacities. For species i, the molar enthalpy may be expressed as $h_i = h_i^0 + \widetilde{h}_i(T)$ where h_i^0 is the heat of formation, $\widetilde{h}_i$ is the sensible enthalpy and T is the temperature. The heat of formation is taken at the above reference conditions, giving $\widetilde{h}_i = \int_{T_{ref}}^{T} C_{p,i} dT$ where $C_{p,i}$ is the molar constant-pressure heat capacity. A heat of combustion for species i is given by

$$h_i^c = h_i^0 - \sum_j w_{ji} h_j^0 \tag{9}$$

under the assumption that water remains in vapor state. The energy equation is

$$\left(N_c C_{p,h} + \sum_{i \in lights} C_{p,i} N_i \right) \frac{dT}{dt} =$$

$$- \sum_{i \in lights} h_i \mathcal{R}_i + N_c (R_u T_{ref}) K_h \tag{10}$$

where

$$\mathcal{R}_i \equiv (dN_i/dt)_{reac}, \tag{11}$$

R_u is the universal gas constant,

$$C_{p,h} \equiv (\sum_{l \in heavies} C_{p,l} N_l)/N_c, \tag{12}$$

and the rate of enthalpy change due to heavy species l chemical kinetic changes is defined as

$$K_h \equiv - \left(\sum_{l \in heavies} h_l \mathcal{R}_l \right) \frac{1}{R_u T_{ref} N_c}. \tag{13}$$

2.2. Light species as part of the base

Light species are not subject to meaningful decomposition according to the above procedure. Examination of runs made using the LLNL database indicate that the light species should be categorized in two subsets. The species in the first subset require rate equations and are part of the base set. The species in the second subset have a quasi-steady behavior and require fits of their mole fraction value as a function of the state variables (T, N^*, ϕ) and modeling parameters (here, only T_s). This first subset consists of: H_2O, CO_2, O_2, H, CO, H_2, CH_4, H_2O_2, C_2H_2, C_2H_4, CH_2O. The second subset are the radicals: O, CH, CH_2, CH_3, HO, HCO, HO_2, HC_2, C_2H_3. Thus this entire set consists of 20 light species. For their energetics, values of h^c are fitted from the literature and C_p's are obtained as

$$C_p/R_u = a^h + b^h \ln(T/T_{ref}). \tag{14}$$

Other properties of the light molecules and light free-form of the constituent radicals are given in Table 1 [4–7].

2.3. Final base set

The reaction base set is composed of a global (i.e. total) constituent radical and 11 light molecules or free radicals of the first subset (Table 1). Thus, there are only 12 progress variables. To compute N_c one must model K_c; to compute the 11 light species, one must model the KG_i, the KL_i, the X_i of the second subset and the conventional light species reaction rates of the first subset.

3. Results

3.1. Identification of a self-similar behavior

Showing the appropriateness of the scaling with θ rather than using T, the evolution of N_c scaled by $(\phi \times N^*)$ for fixed p_0 at several ϕ values and at fixed ϕ for several p_0 values is illustrated in Fig. 1 using the LLNL kinetics. The normalization attainable with θ scaling is clear and so is the fact that $N_c/(\phi \times N^*)$ is a similarity variable. At fixed $p_0 = 20$ bar, Fig. 1a, all $N_c/(\phi \times N^*)$ curves coincide nearly on the same curve, with the somewhat dissenting curve for $\phi = 4$ showing that for very rich mixtures there are indeed constituents left after the oxidizer was depleted. However, even for as rich a mixture as $\phi = 2$, similarity holds, making this model valid in realms beyond those in advanced reduced schemes [8] where the upper limit of the scheme validity is $\phi = 1.5$, at most [9] $\phi = 2.0$ or exceptionally [10] $\phi = 3$. The behavior in Fig. 1a is typical of all fixed p_0 plots. In Fig. 1b, corresponding plots at stoichiometric conditions are shown, which are generic of all fixed ϕ plots. Again, the similarity achieved with the two normalized variables is remarkable, and only at a combination of high p_0 values and small T_s values (typical of the lowest T limit at which K_c rates are finite), are small to moderate departures from the excellent normalization perceptible.

We note that by $\theta \simeq [0.55, 0.6]$, $N_c \simeq 0$, meaning that modeling errors past that θ range are somewhat irrelevant to the model's accuracy since the reaction is practically finished. Although it would be tempting to curve fit dN_c/dt from Fig. 1 and adopt it as a representative kinetic rate, the fact is that the scaling hides the precise detailed formulation that is required for a sufficiently accurate kinetics to predict T. Thus, fits for K_c are instead needed to achieve appropriate accuracy, as discussed below.

3.2. Global constituent molar density model

Plots of K_c versus θ show that there are two different regions of the curve. For small θ values, there is a combustion incubation region, with reaction times values in ms units. As θ increases, one encounters the fast reaction region with reaction times values in μs units. Numerous tests made with the LLNL kinetics showed that K_c represents only a small difference between production and loss rates which are nearly equal (not shown) and are much larger than K_c. The K_c value is typically about 1.5% to 5% of

either production or loss rate. The maximum difference between production and loss rates is about 5% for $N^* \lesssim 1$, then decreases to about 3% at larger N^*. These maximum differences tend to occur during very large values of dT/dt. This fact suggests that K_c could be treated as a rate of a nearly quasi-steady process. If fits of K_c can be obtained over a significant region of parametric behavior, this model would be compact and represent a considerable reduction in the problem dimensionality. Noteworthy, had the approach been to find K_c from slopes of N_c in Fig. 1, it is clear that the important incubation region would have been missed.

Fitting K_c as a function of T and parameters N^*, ϕ and T_s presented a major challenge because of the non-monotonic K_c behavior and also because K_c spans so many decades. Fits were obtained by first inspecting the LLNL kinetics to understand the rate constant, K, variation. This variation showed an incubation region ($\theta \leq 0.2$) featuring first a maximum, K_{mx}, followed by a minimum, K_{mn}, and a high-T region ($\theta > 0.2$) where K_c monotonically increases. Thus, the functional fits are performed in three separate regions, with connection constraints between consecutive regions (the ultimate fits are piecewise continuous). The non-monotonic incubation-region behavior is captured by using a cubic functional mapping from $K(T)$ to $y(T)$ through the form

$$K(T) = \frac{1}{2}(K_{mx} + K_{mn})$$

$$+\frac{1}{4}(K_{mx} - K_{mn})(y^3 - 3y) \qquad (15)$$

where $y(T) = -1$ at $T = T_{mx}$ which is the location of K_{mx} and $y(T) = 1$ at $T = T_{mn}$ which is the location of K_{mn}. In fact, the range of y is from slightly smaller than -2 at $T = T_s$ (i.e. $K_c > 0$) to $y \lesssim 1.8$. The values of K_{mx}, K_{mn}, T_{mx} and T_{mn} are fitted as polynomials in parameters $\ln(N^*), \ln(\phi)$ and $\ln(T_s/T_{ref})$. Also fitted is T_0 which is the T value at which $y = 0$. Two different changes of variables are made from $y(T)$ to $y(z)$ depending on how T compares to T_0. For $T < T_0$, a variable $z \equiv (T_0 - T)/(T_0 - T_{mx})$ is defined, which means that $y = -1$ at $z = 1$. To achieve the mapping, we first generate (y, z) pairs which are functions of parameters $\ln(N^*), \ln(\phi)$ and $\ln(T_s/T_{ref})$. To match these pairs, a ratio of appropriate functions (e.g. polynomials $a + bz + cz^2 + ...$; power functions of type a^z; and combinations of the two functional forms) is chosen to produce the $y(z)$ mapping. For $T > T_0$, i.e. $y \geqslant 0$, a similar procedure is used for $y(z)$ where now $z \equiv (T - T_0)/(T_{mn} - T_0)$. Beyond incubation, for the high-T region, $\ln(K)$ is fitted as a fifth order polynomial in θ^p where $p = 1$ for $\phi \leqslant 0.5$ and $p = (0.86 + 0.28\phi)/(0.74 + 0.52\phi)$ for $\phi > 0.5$. Scrutiny of the LLNL kinetics showed that the largest value of T_s is 825 K. Then, for $T_s = 825$ K, the polynomial coefficients were fitted, separately for the lean/stoichiometric ($\phi \leqslant 1$) and rich ($\phi > 1$) regions, as polynomials in $\ln(N^*)$ and $\ln(\phi)$. To obtain fits for $T_s < 825$ K, a scaling procedure was used from the $T_s = 825$ K fits to match particular K values at a specific point in the incubation region.

All fits further presented in Figs. 2-6 have been achieved with the fixed set of mapping functions described above. That is, no local corrections of any sort were used, nor exceptions from those functions were considered. Local corrections in a four-dimensional space are not computationally practical.

Curve fits to K_c computed using the LLNL kinetics are plotted in Figs. 2-4. In Fig. 2a and 2b (fixed p_0, various ϕ and T_s), and Fig. 3a and 3b (fixed ϕ in the lean regime, various p_0 and T_s) we differentiate between the incubation and fast-reaction regions discussed above and show on each figure up to 5 decades of kinetic rates. On each figure, symbols represent the LLNL-based computation and the symbol location represents a selected sample of time stations during the calculation. The curve fits are shown as lines and are based on time stations at fixed intervals of $\Delta\theta$. The agreement on the logarithmic scale is excellent to very good and deterioration of the fits at $\theta \gtrsim 0.55$ correspond to very small values of N_c, as noted above. Particularly important is the excellent agreement between fits and LLNL kinetics in the region of $\theta \leq 0.2$ representing 54% of the N_c decay (see Fig.1). For $\theta > 0.2$ the agreement is still excellent as long as T_s is not too low; good agreement still occurs in the significant N_c regions (i.e. $\theta \lesssim [0.55, 0.6]$) and over a much wider ϕ range than usually shown in the literature. Figure 4a focusses on the rich regime, showing the entire range of relevant θ (see Fig. 1a) at various p_0 and T_s. The agreement of fits with the LLNL data is excellent, bodying well for future studies addressing soot and CO formation. Noteworthy, the fits encompass a wide p_0 range including the desired high-pressure situations for engine combustion, and a much wider ϕ range than typically used in kinetic reduction schemes [8] where generally $\phi \in [0.5, 1.5]$, sometimes [9] $\phi \in [0.5, 2.0]$ and exceptionally [10] $\phi \in [0.7, 3.0]$. To show the influence of T_s, in Fig. 4b is depicted the case for which the widest range of T_s was available, corresponding to $p_0 = 10$ bar and $\phi = 1$. Similar to the other figures, the agreement with the LLNL kinetics is excellent to very good up to $\theta \leq 0.2$ and somewhat deteriorates past that station.

This deterioration is a manifestation of the need for matching two different functional forms: one in the incubation region ($y > 0$), and the other in the high-T region. The matching point is at $y_{\max}$; as $y_{\max}$ increases, the high-T region fit improves while the incubation fit worsens, and vice versa for decreasing $y_{\max}$. Fits can also be improved if one is less ambitious in covering the large ϕ range treated here. The functional behavior of ϕ outliers is somewhat different from that for moderate ϕ. For $\phi < 1$ and small, the high-T rates are quite modest and below K_{mx}. For $\phi > 1$, as ϕ increases, the ratio K_{mx}/K_{mn} decreases and high-T rates exceed K_{mx} except for the largest ϕ

where the reaction terminates before the K_{mx} value is reached again in the high-T region. This behavior is independent of p_0. This is to say that if the ϕ outliers are eliminated, a much simpler picture arises and consequently more accurate fits are possible. Conceptually, one could also improve the fits by using a larger number of parameters in the model, however, this would defeat the purpose of computational efficiency that is the basis for seeking reduced kinetics.

3.3. Recovery of the energetics

According to eq. 10, to recover the value of T in the reduction scheme, the heavy species model should focus on an appropriate representation of $C_{p,h}$ and K_h. Plots (not shown) of $C_{p,h}$ at various p_0 values, calculated using the LLNL model over a wide range of ϕ, show that these curves exhibit a very modest variation over the range of strong N_c decay; moderate (i.e. up to 50%) variation occurs only after N_c values are very small to negligible. This indicates that the T recovery is primarily governed by K_h as far as heavy species modeling is concerned.

Examples of K_h model fits to the LLNL calculated values are shown in Figs. 5 and 6. First, it is clear that the plots resemble functionally those of K_c, which is not surprising given the definitions of eqs. 3 and 13. Second, the energetics is remarkably well recovered for a variety of ϕ and T_s (Fig. 5), including very rich mixtures (Fig. 6). Similarly, excellent to very good results are obtained for lean mixtures (not shown). Should more accurate K_h fits be desirable, the K_c discussion on this topic is entirely pertinent.

4. Completing the kinetic model

Brevity does not permit the detailed discussion of the remaining kinetic-model parts, but the process to complete the model is clear. What remains to be done is the fitting of quasi-steady gain rates KG_i (where i stands for H_2O, CO_2, O_2, H, CO, H_2, CH_4, H_2O_2, C_2H_2, C_2H_4, CH_2O), of quasi-steady loss rate KL_i (where i stands for H_2O, O_2, H, H_2, this rate being null for the other light species) and of the quasi-steady light species mole fraction X_i. To show that the K_c fitting has set a methodology for completing the model, displayed in Fig. 7 is the quasi-steady rate function KG for CO at p_0 = 30 bar. The plot was obtained using the LLNL kinetics. Function KG_{CO} represents the net gain of molar density N_{CO} due to all rates involving the heavy species group (note: KL_{CO} is null). The plot graphically resembles K_c and K_h, indicating a consistent quasi-steady functional behavior for the heavy group contribution similar to that previously identified for K_c. Moreover, with increasing ϕ beyond $\phi = 1$, an asymptotic self-similar behavior is evident in the fast reaction regime. This plot is typical of all KG_i rates and shows that the same fitting methodology used for K_c and K_h will apply.

Regarding the rates KL_i (except for possibly $i =$ H), they also have the specific graphical form (not shown) seen for K_c, K_h and KG_{CO}; thus, for constructing KL_i and X_i fits, the same basic fitting methodology will apply as for K_c and K_h.

5. Conclusions

The LLNL heptane kinetic model has been examined focussing on a potential very computationally efficient kinetic reduction scheme. Species were categorized into light or heavy (C number $n \geqslant 3$). The heavy species were decomposed into defined 13 constituents, and it was shown that a non-dimensional temperature θ depending on the pressure variable N^* and the equivalence ratio ϕ can be defined so that the ratio of the total constituent molar density N_c to the product of equivalence ratio and a nondimensional pressure N^* exhibits a self-similar behavior over a wide range of initial p_0, ϕ and a model-defined temperature T_s entering the computation of θ. The number of progress variables is thus reduced from 160 progress variables to 12 (11 for perfectly stirred reactor cases where H is also quasi-steady): the unsteady light species and N_c.

Assessment of the total constituent reaction rate, K_c, behavior revealed that it is quasi-steady and features two distinct regimes: incubation and fast reaction. The rate was fitted in terms of a total of four parameters: the physical parameters T or θ (a surrogate for T), ϕ, N^* and a modeling parameter T_s; θ itself is a function of ϕ, N^* and T_s. The same functions were used to achieve the fits over the entire region covered by the four parameters. These plots reproduced with excellent to very good accuracy the reaction rate over the significant lifetime of the total constituent and for a range of p_0 and ϕ that is much wider than the typical one used for displaying reduced mechanisms. The energetics associated with the heavy species reaction rate, K_h, was also recovered through fits which were functionally similar to those for K_c. Expectably, it is found that the K_h value rather than the value of the heavy species heat capacities at constant pressure, $C_{p,h}$, contributes mostly to the enthalpy change associated with the heavy species reaction. The $C_{p,h}$ also requires fitting. Mathematically, the shown fits achieved substantial accuracy over seven rate decades considering the fact that they depend upon four variables.

The model is completed once the gain/loss of light species molar density from the heavy species and the mole fraction X_i (relative to the light group) of quasi-steady light species are fitted. Examination of these gain/loss rates shows that they also have a quasi-steady behavior. As an example, it was shown that the gain-rate functional form with respect to θ emulates those of K_c and K_h, making the modeling strategy clear. This finding highlights the fact that the fitting technique provides a methodology which can be repeatedly used to obtain an accurate representation of full or skeletal kinetic models. The advantage of the proposed model is that the kinetic reduction is performed before embedding the kinetics in a turbulent flow computation and would be used as a library of

rates rather than needing 'on-the-fly' kinetic rate calculations.

To summarize, the proposed reduced model features 12 ultimate progress variables describing heptane oxidation. The reduced model requires fitting 16 quasi-steady rate functions, 11 curves for light quasi-steady mole fractions, and $C_{p,h}$. Also required are conventional rates between members of the light group, which are available in the literature. Because this model is based on the N_c rate rather than on that of individual heavy species, even if the number of species increases with increased C number in the alkane group, providing that the quasi-steady rate aspect persists, then extension of this model to higher alkanes should be conceptually straightforward; although it remains to be seen if the functional fits would remain valid or would require reconstruction.

Acknowledgments

This study was conducted at the Jet Propulsion Laboratory (JPL), California Institute of Technology (Caltech) and sponsored at Caltech by the Army Research Office under the direction of Drs. David Mann, Kevin McNesby and Ralph Anthenien.

References

[1] Lawrence Livermore National Laboratory,http://www-cms.llnl.gov/combustion/combustion2.html.
[2] S. W. Benson, Thermochemical Kinetics., John Wiley & Sons, Inc., 1968.
[3] R. C. Reid, J. M. Prausnitz, B. E. Poling, *The Properties of Gases and Liquids* (1987) McGraw-Hill Book Co., 4th edition, Chapt. 6.
[4] National Institute of Standards and Technology, Chemistry WebBook; http://webbook.nist.gov/chemistry/.
[5] CRC Handbook of Chemistry and Physics, 86th Ed., D. R. Lide, Ed.-in-chief, CRC Press, Boca Raton, Fl., 2005 (internet edition).
[6] Gas Research Institute, http://www.me.berkeley.edu/gri-mech/.
[7] NASA Glenn Research Center, http://cea.grc.nasa.gov/.
[8] T. Lu, C. K. Law, *Combust. Flame*, 144 (2006) 24-36.
[9] N. Peters, G. Paczko, R. Seiser, K. Sheshadri, *Combust. Flame*, 128 (2002) 38-59.
[10] V. I. Babushok, W. Tsang, *J. Propul. Power*, 20(3) (2004) 403-414.

Mo/Ra	h^0	h^c	a^h	b^h
H_2	0.0	241.5	3.282	0.400
O_2	0.0	0.0	3.476	0.5663
N_2	0.0	0.0	3.388	0.469
C	717	1111	2.50	0.0
H_2O	-241.5	0.0	3.688	1.217
CO_2	-393.5	0.0	4.690	1.390
N	473	473	2.50	0.0
H	218.0	339	2.50	0.0
HO	38	159	3.385	0.3637
HOO	10.5	131	4.150	1.307
O	249.2	249.2	2.536	0.0
CO	-110.5	283	3.426	0.4749
HCO	43.1	558	4.154	1.2875
CH_4	-74.6	802	3.797	4.305
CH_3	146	902	4.440	2.249
CH_2	390	1025	3.973	1.3015
CH	596	1110	3.220	0.7136
C_2H_3	300	1449	5.1	3.5
HC_2	566	1474	4.434	1.404
C_2	838*	1625	4.58	0.0
NO	90.3	90.3	3.533	0.4508
NO_2	33.2	33.2	4.691	1.151
H_2O_2	-136	106	5.269	1.880
HCOH	-109	526.5	4.27	2.546
C_2H_2	228	1257	5.368	2.294
C_2H_4	52.5	1323	5.383	4.676

*Alternate value of 832 from the CRC tables.

Table 1: Thermodynamic properties of molecules and free radicals. h^0 and h^c (heats of formation and combustion, respectively), in kJ/mol; constants a^h and b^h for molar heat capacity in the form $C_p/R_u = a^h + b^h ln(T/T_{ref})$; T_{ref} = 298.15 K. "Mo" denotes "molecule". "Ra" denotes "radical".

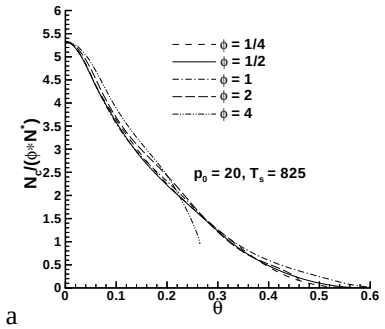

a

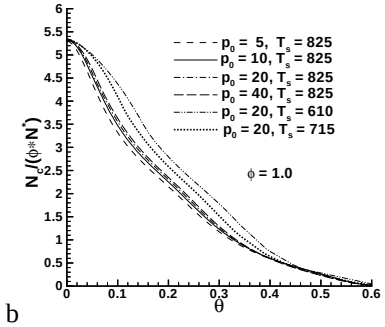

b

Fig. 1: Similarity plots of parameter $N_c/(\phi \times N^*)$ versus θ at (a) $p_0 = 20$ bar and (b) $\phi = 1$. T_s is in K.

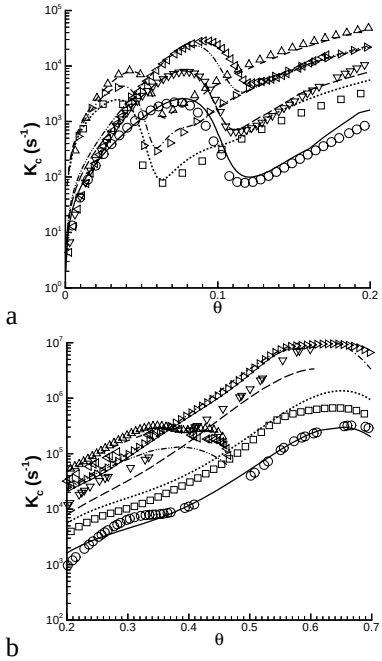

Fig. 2: K_c versus θ for $p_0 = 20$ bar. Symbols $\square$, $\triangleright$, Δ, $\bigcirc$, ∇, $\triangleleft$ represent selected data from the LLNL runs; lines $\bullet\bullet\bullet$, $-\bullet-\bullet-\bullet-$,- - -, ——, $-\,-\,-$, $-\bullet\bullet-\bullet\bullet-$ represent the corresponding fits. Temperatures units are in degrees K. The legend is: $\bullet\bullet\bullet$ $\phi = 0.5, T_s = 825$; —— $\phi = 0.5, T_s = 715$, $-\bullet-\bullet-$ $\phi = 1.0, T_s = 825$; $-\,-\,-$ $\phi = 1.0, T_s = 715$; - - - $\phi = 2.0, T_s = 825$; $-\bullet\bullet-\bullet\bullet-$ $\phi = 2.0, T_s = 715$.

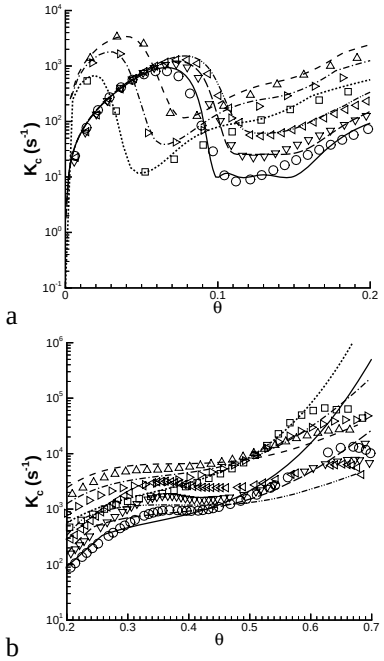

Fig. 3: K_c versus θ for $\phi = 1/3$ at different p_0 and T_s. Symbols $\square$, $\triangleright, \Delta, \bigcirc, \nabla, \triangleleft$ represent selected data from the LLNL runs; lines $\bullet\bullet\bullet, -\bullet-\bullet-$,- - -, ——, $---, -\bullet\bullet-\bullet\bullet-$ represent the corresponding fits. Units: pressures in bar, temperatures in degrees K. The legend is: $\bullet\bullet\bullet$ $p_0 = 10, T_s = 825$; —— $p_0 = 10, T_s = 715$, $-\bullet-\bullet- p_0 = 20, T_s = 825$; $---$ $p_0 = 20, T_s = 715$; - - - $p_0 = 40, T_s = 825$; $-\bullet\bullet-\bullet\bullet- p_0 = 40, T_s = 715$.

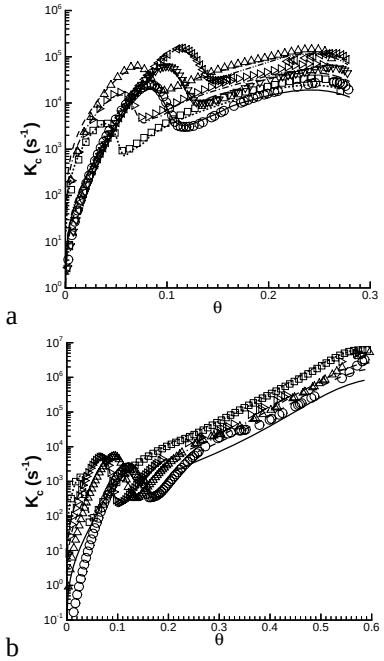

Fig. 4: K_c versus θ for a variety of conditions. Symbols $\square$, $\triangleright$, Δ, $\bigcirc$, ∇, $\triangleleft$ represent selected data from the LLNL runs; lines $\bullet\bullet\bullet$, $-\bullet-\bullet-$,- - -, ——, $---$, $-\bullet\bullet-\bullet\bullet-$ represent the corresponding fits. Units: pressures in bar, temperatures in degrees K. (a) $\phi = 4$, ($\bullet\bullet\bullet$ $p_0 = 10$, $T_s = 825$; —— $p_0 = 10$, $T_s = 715$, $-\bullet-\bullet-$ $p_0 = 20$, $T_s = 825$; $---$ $p_0 = 20$, $T_s = 715$; - - - $p_0 = 40$, $T_s = 825$; $-\bullet\bullet-\bullet\bullet-$ $p_0 = 40$, $T_s = 715$). (b) $p_0 = 10$ and $\phi = 1$ ($\bullet\bullet\bullet$ $T_s = 825$; —— $T_s = 715$, $-\bullet-\bullet-$ $T_s = 655$; $---$ $T_s = 560$).

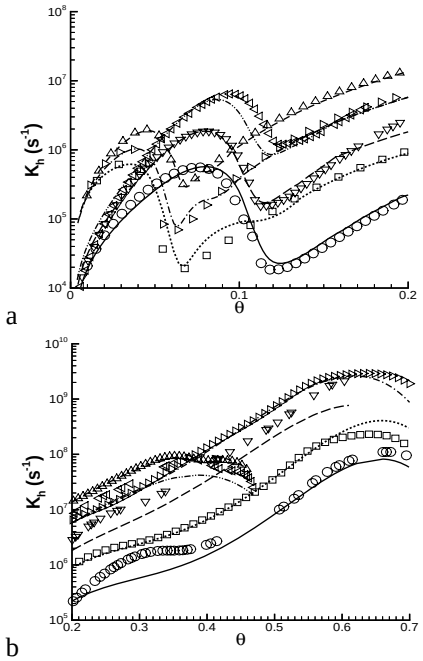

Fig. 5: K_h versus θ at fixed $p_0 = 20$ bar for different ϕ and T_s values corresponding to (a) Fig. 2a, and (b) Fig. 2b. The legend is in Fig. 2 caption.

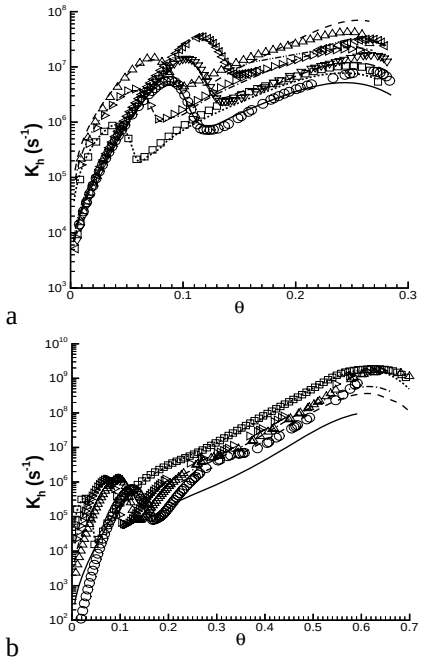

Fig. 6: K_h versus θ for (a) $\phi = 4$ corresponding to Fig. 4a, and (b) $\phi = 1$ and $p_0 = 10$ bar corresponding to Fig. 4b. The legend is in Fig. 4 caption.

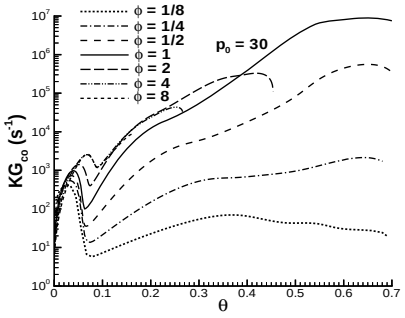

Fig. 7: KG for CO versus θ. p_0 is in bar. Plots obtained using the LLNL data in CHEMKIN II.

APPENDIX 4

Modeling of Alkane Oxidation using Constituents and Species

Kenneth G. Harstad[♦,*] and Josette Bellan[♦,**,†]
Jet Propulsion Laboratory[♦], *California Institute of Technology, Pasadena CA 91109-8099*
California Institute of Technology[**], *Mechanical Engineering, Pasadena, CA 91125*

A chemical kinetics reduction model is proposed for alkane oxidation in air that is based on a parallel methodology to that used in turbulence modeling in the context of Large Eddy Simulation. The objective of kinetic modeling is to predict the heat release and temperature evolution. In an *a priori* step, a categorization of time scales is first conducted to identify scales that must be modeled and scales that must be computed using progress variables based on the model for the other scales. First, a decomposition of heavy (carbon number greater or equal to 3) hydrocarbons into constituents is proposed. Examination of results obtained using the LLNL heptane-oxidation database in conjunction with Chemkin II shows that (i) with appropriate scaling, the total constituent mole fraction behaves in a self-similar manner and the total constituent molar density rate follows a quasi-steady behavior, and (ii) the light species can be partitioned into two subsets according to whether they are quasi-steady (nine species) or unsteady (11 species). The twelve progress variables represented by the total constituent molar density and the molar densities of the unsteady light species are defined to be a base from which the system's behavior can be reproduced. This is a dramatic reduction from the 160 species (progress variables) and 1540 reactions in the LLNL set to 12 progress variables, 16 quasi-steady rates (associated with heavy species), 162 conventional reaction rates (light species) and 11 other functional forms (i.e. fits for the mean heavy-species heat capacity at constant pressure, the enthalpy release rate of the heavy species, and the molar fraction of quasi-steady light species). A summary of the model is presented explaining the curve fits that constitute the model, namely (1) for the constituent molar density rate along with the corresponding enthalpy production rate, (2) for the quasi-steady species mole fraction, and (3) for the contribution from the heavy species to the unsteady light species reaction rates. The proposed kinetic mechanism is valid over a pressure range from atmospheric to 60 bar, temperatures from 600 K to 2500 K and equivalence ratios from 0.125 to 8. This range encompasses diesel, HCCI and gas turbine engines, including cold ignition; and NO_x, CO and soot pollutant formation in the lean and rich regimes, respectively. Highlights of the *a priori* model results are illustrated for a variety of initial conditions. Results from *a posteriori* tests are shown in which the model predictions for the unsteady light species and the temperature are compared to the equivalent quantities based on the LLNL dataset.

I. Introduction

The challenge of modeling turbulent reactive flows is so considerable that the activity has traditionally been decomposed in its two essential parts: kinetics and turbulence. Traditionally, modeling of chemical kinetics has proceeded on a separate path from that of turbulence which also includes canonical models for turbulence/reaction interaction. The only constraint to kinetic modeling was that it should be compact enough to be computationally efficient when included in a complex turbulent combustion code. However, there are definite advantages on approaching chemical kinetic modeling in a similar manner to turbulent flow

[*]Senior Engineer.
[†]Senior Research Scientist, AIAA Fellow (corresponding author, josette.bellan@jpl.nasa.gov).

modeling because if the concepts are similar, the hope is that the models will mesh better and the results will be easier to understand. This is the approach taken here. The spirit of the chemical kinetic modeling approach is that of Large Eddy Simulations (LES) in which kinematically energetically-significant flow scales are computed and the others are modeled; in turbulence, the large flow scales constitute the former category and the small flow scales constitute the latter category. The chemical kinetics parallel is to obtain a model in which one retains only the thermodynamically energetically-significant chemical scales as progress variables and models the fate of the other scales. But the parallel approach between kinetics and turbulence can go even further. In turbulence modeling, a common methodology is to assess the behavior of the modeled scales by analyzing databases created using Direct Numerical Simulations (DNS) in which all flow scales are computed; indeed, current experimental diagnostics do not permit the same thoroughness of information as that obtained from DNS. The DNS data is analyzed in what is called an *a priori* study to inquire about the behavior of the small scales and propose mathematical forms which fit this behavior. The *a priori* study is followed by an *a posteriori* study where the proposed mathematical forms are inserted into the model to evaluate its performance when compared to the DNS database at the LES resolution.

A complete analogy between turbulence and kinetics can be made by observing that kinetic elemental or skeletal mechanisms can serve for reduced kinetics the role that DNS serves for LES, in which case reduced kinetic mechanisms can be viewed as the complement to LES in achieving the goal of accurate computationally-efficient turbulent reactive flow simulations. The analogy between reduced kinetic models and LES is not entirely surprising since each chemical species has a characteristic time scale and in the kinetic reduction it is desirable to compute only those entities (e.g. species, combination of species, radicals, combination of radicals, etc.) having an essential characteristic time scale (to be defined) and model the kinetics of the remaining entities.

Thus, there are two important components to this study, namely the *a priori* analysis and the *a posteriori* evaluation. Whereas turbulence modeling benefits from decades of work using the DNS/LES concept which originated in atmospheric turbulence predictions in the 1960s, the present work is the first investigation to take this approach in kinetic reduction modeling. Therefore, it is first necessary to produce a categorization of scales analogous to the large and small scales of turbulence, then it is required to propose mathematical forms for the scales that will be modeled rather than computed as progress variables in the reduced kinetic model, and finally it is required to perform an *a posteriori* study in order to evaluate the chemical kinetic model versus the elemental or skeletal mechanism for those species predicted by the reduced model. The present model is for a constant-volume situation, so as to be consistent with the requirement of a LES grid.

In Section II we propose such a categorization through the definition of a total constituent radical and the partition of the light species set into a set of modeled species and a set of progress variable species. That is, rather than following all species through their reaction coordinates, we follow a reduced set of reaction coordinates (i.e. progress variables); this reduced set is called a base. Section III is devoted to the *a priori* model. In Section IV, the behavior of the base set is briefly examined *a priori* in the context of a detailed reaction model for n-heptane combustion as given by LLNL,[1] and the proposed mathematical forms are tested against the LLNL kinetic scheme; some *a priori* results were previously described in more detail[2] and we only give here highlights of the model and results that were not previously available. Section V is devoted to a limited *a posteriori* evaluation of the model. Finally, in Section VI a summary of the accomplishments and a perspective on future work are offered.

II. Categorization of chemical scales

The categorization of scales into modeled and computed is produced for the primary objective of the accurate determination of the energetics, i.e. heat release and temperature evolution; at this initial stage of model development, neither NO_x nor soot kinetics are addressed. All species involved in hydrocarbon oxidation are partitioned into light species or heavy species; the heavy species are those having a carbon number $n \geqslant 3$. The proposed model is for alkane combustion using as a template the n-heptane LLNL[1] data mentioned above. Thorough examination of the results using the data led to the following proposed representation. The heavy species' rate evolution is modelled, resulting in a single progress variable constructed as the total constituent radical molar density of the heavy species, as defined in Section IIIA. The light species set is composed of two subsets: the first subset is that of species characterized by a quasi-steady behavior which is modeled, and the second subset is that of unsteady species which are computed as progress variables, both of which are described in Section IIIB. That is, rather than computing all species through

their reaction coordinates, a reduced set of reaction coordinates is computed that contains an aggregate resulting from the heavy species decomposition and the unsteady light species. This reduced set is called a base.

III. *A priori* modeling and the resulting conservation equations

The *a priori* model addresses all heavy species and some of the light species (i.e. all quasi-steady light species).

A. Heavy species: the total constituent model as progress variable

Consider the count of atoms (H,C,O,N) in species i. We define w_{ji} as the number of species j in species i that produces the correct atom count, where the index j denotes the species set of air (O_2,N_2) and final combustion products (H_2O,CO_2). (This means that mathematically, we consider species i as being composed of air and final combustion product species.) The molar densities of species in this set are

$$N_j = N_j^0 - \sum_{i \neq j} w_{ji} N_i \tag{1}$$

where N_j^0 is the effective total molar density of species j. The same exercise of atom counting and species representation by the j set can be performed for all species in the mixture to obtain N_j^0. That is, the atomic elements molar densities are represented by species j molar densities. Conservation of atoms in the reactions makes unnecessary utilizing rate expressions for reaction coordinates of air species and complete-combustion products, as a one-to-one map exists between these and the atom set. The heavy species constituent radicals (CH_2, CH_3, CH, C_2H_3, C_2H_2, C_2, HC_2, CO (keto), HCO, HO, HO_2, OO, O) form a set of 13 entities from which any heavy species or radical may be constructed. The total constituent molar density is

$$N_c \equiv \sum_{k=1}^{13} N_k \tag{2}$$

where the molar density of constituent k is N_k. The decomposition into constituents is similar to group additivity,[3,4] except that it considers only first order (compositional) effects and only interactions with adjacent groups. The reaction rate associated with N_c is defined by

$$K_c \equiv -\frac{d(\ln N_c)}{dt}. \tag{3}$$

We define a reference density for nitrogen N_2 from the dry air value at pressure $p_{ref} = 1$ bar and T_{ref}= 298.15 K, giving N_{ref}= 31.5 mol/m^3. Using N_{ref}, a dimensionless N_2 molar density is defined as

$$N^* \equiv \frac{N_{N2}}{N_{ref}} \tag{4}$$

which acts as a convenient surrogate variable for the pressure p as the N^* value is essentially rate invariant. That is, the partial pressure of N_2 is the overwhelming contribution to p. Basically, the ratio of N^* to p_0 is nearly constant. A normalized temperature variable θ is defined by

$$\theta \equiv \frac{T - T_s}{T_r(\phi, N^*)} \tag{5}$$

$$T_r \equiv 2065 (N^*)^{0.06} w(\phi) \tag{6}$$

$$w(\phi) = \phi \frac{1.5 + 1.31\phi}{1 + 0.71\phi + 1.1\phi^2} \tag{7}$$

where T_s is a modeling parameter representing the lowest temperature at which $K_c > 0$. The θ definition is such that N_c decreases during stoichiometric combustion from its initial value by three orders of magnitude (delving into higher order of magnitude decrease runs the risk of encountering round-off and truncation errors) for $\theta \gtrsim 0.6$, a value chosen so that all θ values remain below unity for all test case calculations.

B. Light species: a modeled subset and a progress variable subset

Light species are not subject to meaningful decomposition according to the above procedure. All light species are listed in Table 1. Examination of runs made using the LLNL database in Chemkin II indicates that the light species should be categorized in two subsets: one which is modeled and one which is computed subject to the heavy species model.

1. Modelled light species

The species in the first subset are the radicals O, CH, CH_2, CH_3, HO, HCO, HO_2, HC_2, C_2H_3 which have a quasi-steady behavior and require mathematical fits of their mole fraction value as a function of the state variables (T, N^*, ϕ) and modeling parameters (here, only T_s). There are nine of these species.

2. Progress variable light species

The species in the second subset require rate equations. This set consists of H_2O, CO_2, O_2, H, CO, H_2, CH_4, H_2O_2, C_2H_2, C_2H_4, CH_2O. The contribution of the heavy group to the rate of change of a light species molar density N_i with mole fraction X_i (relative to the light group) is expressed in terms of quasi-steady gain and loss rates KG_i and KL_i as

$$\left.\frac{dN_i}{dt}\right|_{heavies} = N_c(KG_i - X_i KL_i) \tag{8}$$

where KG_i and KL_i must be modeled consistently with the heavy species model. There are eleven of these species.

C. Model summary for species and computation of energetics

The base set is composed of a global (i.e. total) constituent radical and 11 light molecules or free radicals of the second light species subset. Thus, there are only 12 progress variables. To compute N_c one must model K_c. To compute the 20 light species, one must model X_i of the first light species subset and compute the conventional light species reaction rates of the second light species subset for which models of KG_i and KL_i are needed consistent with the fact that the heavy species do not appear explicitly but rather through the total constituent N_c.

Aside from the molar reaction rates, determining the temperature evolution in a reactive system requires knowledge of the species molar enthalpies and heat capacities. For species i, the molar enthalpy may be expressed as $h_i = h_i^0 + \widetilde{h}_i(T)$ where h_i^0 is the heat of formation, $\widetilde{h}_i$ is the sensible enthalpy and T is the temperature. The heat of formation is taken at the above reference conditions, giving $\widetilde{h}_i = \int_{T_{ref}}^{T} C_{p,i} dT$ where $C_{p,i}$ is the molar constant-pressure heat capacity. A heat of combustion for species i is given by

$$h_i^c = h_i^0 - \sum_j w_{ji} h_j^0 \tag{9}$$

under the assumption that water remains in vapor state. The energy equation is

$$\left(N_c C_{p,h} + \sum_{i \in lights} C_{p,i} N_i\right) \frac{dT}{dt} = -\sum_{i \in lights} h_i \mathcal{R}_i + N_c (R_u T_{ref}) K_h \tag{10}$$

where

$$\mathcal{R}_i \equiv \left(\frac{dN_i}{dt}\right)_{reac} = \left.\frac{dN_i}{dt}\right|_{heavies} + \left.\frac{dN_i}{dt}\right|_{lights}, \tag{11}$$

R_u is the universal gas constant,

$$C_{p,h} \equiv \frac{\left(\sum_{l \in heavies} C_{p,l} N_l\right)}{N_c}, \tag{12}$$

and the rate of enthalpy change due to heavy species l chemical kinetic changes is defined as

$$K_h \equiv -\left(\sum_{l \in heavies} h_l \mathcal{R}_l\right) \frac{1}{R_u T_{ref} N_c}. \tag{13}$$

Clearly, since K_h is associated with the heavy species, it must be modeled.

For the energetics, values of h^c are fitted from the literature and C_p's for the light species are obtained as

$$\frac{C_p}{R_u} = a^h + b^h \ln\left(\frac{T}{T_{ref}}\right). \tag{14}$$

Other properties of the light molecules are given in Table 1.[5–8]

IV. Highlights of *a priori* results

A. Examination of the database using the proposed scaling

One of the most important findings of the categorization of scales identifying N_c as the important dependent variable representing the heavy species is that when N_c is scaled by $(\phi \times N^*)$ and the evolution is followed as a function of θ rather than using T, a self similar behavior emerges for $N_c/(\phi \times N^*)$, as shown in Fig. 1 using the LLNL kinetics. The similarity achieved with the two normalized variables is remarkable, and only at a combination of high p_0 values and small T_s values (typical of the lowest T limit at which K_c rates are finite), are small to moderate departures from the excellent normalization perceptible. Even for as rich a mixture as $\phi = 2$, similarity holds, making this model valid in realms beyond those in advanced reduced schemes[9] where the upper limit of the scheme validity is $\phi = 1.5$, at most[10] $\phi = 2.0$ or exceptionally[11] $\phi = 3$. This self similar behavior can be understood as a reduction in dimensionality of the problem but should not be confused with the intrinsic low-dimensional manifold[12] because that concept was developed for actual chemical species, whereas our findings are for N_c. The fact that N_c can embody the evolution of all heavy species is consistent with, and can be traced to, the fact that as T increases, the heavy species decompose and no longer play a role; instead, the products of this decomposition determine the reaction evolution.

The above findings were for the LLNL data. The *a priori* study is meant to propose models, that is, mathematical forms, for this behavior. This model is briefly described next.

B. Proposed model

Examination of Fig. 1 shows that by $\theta \simeq [0.55, 0.6]$, $N_c \simeq 0$, meaning that modeling errors past that θ range are somewhat irrelevant to the model's accuracy since the reaction is practically finished. Although it would be tempting to curve fit dN_c/dt from Fig. 1 and adopt it as a representative kinetic rate, the fact is that the scaling hides the precise detailed functional form of K_c. For consistency, K_c should be curve-fitted similar to K_h and other reaction rates. These K_c mathematical forms and an assessment of how well they fit the LLNL data were previously described.[2] According to eq. 10, to recover the value of T in the reduction scheme, the heavy species model should focus on an appropriate representation of $C_{p,h}$ and K_h. Plots (not shown) of $C_{p,h}$ at various p_0 values, calculated using the LLNL model over a wide range of ϕ, show that these curves exhibited a very modest variation over the range of strong N_c decay; moderate (i.e. up to 50%) variation occurs only after N_c values are very small to negligible. This indicates that the T recovery is primarily governed by K_h as far as heavy species modeling is concerned. Comparison of the model for K_h, which was essentially similar to that for K_c showed that it fitted remarkably well the results from the LLNL database for a variety of ϕ and T_s, including the difficult to model very rich mixtures.[2]

The model is completed with the fitting of quasi-steady gain rates KG_i (where i stands for H_2O, CO_2, O_2, H, CO, H_2, CH_4, H_2O_2, C_2H_2, C_2H_4, CH_2O), of quasi-steady loss rate KL_i (where i stands for H_2O, O_2, H, H_2, this rate being null for the other light species) and of the quasi-steady light species mole fraction X_i (O, CH, CH_2, CH_3, HO, HCO, HO_2, HC_2, C_2H_3). Selected plots for KG_{H_2} and KG_H are presented in Fig. 2; the ratio $RL_i \equiv KL_i/KG_i$ is illustrated in Fig. 3 for $i = H_2$ and $i = H$; and X_{OH} is depicted in Fig. 4. The model for these three quantities is constructed considering KG_i, RL_i and X_i as functions of T or θ, with N^*, ϕ and T_s as being parameters. Both KG_i and X_i are split into a low T, low-rate portion termed the incubation region ($\theta \leq 0.2$), and a high T, high-rate portion termed the fast-rate region. The incubation region variations exhibit a maximum value of KG_i or X_i followed by a dip to a minimum from which a continuous increase is observed to the fast rate region. Conversely, RL_i first exhibits a minimum, and then a maximum. Curve fits to the incubation region results, obtained using Chemkin II with the LLNL data, are generated utilizing either one of the two following methods. In the first method, sometimes used for KG_i or X_i, one uses a cubic transformation, e.g. $KG_i(T)$ to $y(T)$, such that $y = -1$ at the maximum point and $y = 1$ at the minimum point. Then values of T at fixed y values are fitted in terms of parameters

(N^*, ϕ, T_s); these values then generate the continuous curve $y(T)$ by interpolation of the discrete values. In the second method, the T intervals before the maximum point, between maximum and minimum point and after minimum point are treated separately. Each of these intervals is divided into equal T slices, and logarithm values at slice boundaries are functionally fitted in terms of parameters (N^*, ϕ, T_s). The discrete set of these equally spaced functional forms is used to generate, by polynomial interpolation, the continuous function. This second method is also used sometimes for the high-rate region fits. Alternately, in this region, for a fixed set of (N^*, ϕ, T_s), the logarithm of the function at all input discrete θ values is fitted as a polynomial of θ. The polynomial coefficients are then fitted in terms of (N^*, ϕ, T_s). The choice of the particular method for any i is determined by the overall results obtained in matching the input functions provided by Chemkin II using the LLNL database.

The results in Figs. 2-4 for H_2 and H, as examples, show that even at high pressure, the fits represent the data resonably well. The fits in Figs. 2a and 2b at $T_s = 610$ K display an overestimate of the respective KG in the region $\theta < 0.1$; the model is more accurate as T_s is larger, e.g. Figs. 2e and 2f. For the RL rates, shown for H_2 and H as examples in Fig. 3, misestimates also occur for lower T_s in the $\theta < 0.1$ region (e.g. Figs. 3a and 3b), that are mitigated by the model at larger T_s. The discrepancy betwenn LLNL information and model for $\theta > [0.55 - 0.6]$ is of no concern since by that station $N_c \simeq 0$ (see Fig. 1). Similarly, modeling discrepancies for rich situations are also of no concern past the θ station at which $N_c \simeq 0$.

An example of light species molar fraction fits is shown for OH in Fig. 4, as OH is an important radical which is often identified with the flame location. Over the entire range of T_s, the model duplicates very well the LLNL results.

V. Results of the *a posteriori* study

The developed model is assessed in the *a posteriori* study. The assessment involves comparing the results of the reduced kinetic model for T and the unsteady light species H_2O, CO_2, O_2, H, CO, H_2, CH_4, H_2O_2, C_2H_2, C_2H_4, CH_2O with the predictions of the skeletal LLNL mechanism for n-heptane. Since the LLNL database results using Chemkin II does not compute N_c, an additional computation is here made to calculate this quantity as a diagnostic for the model, with the understanding that it is not a variable that will be of ultimate interest in model predictions. The comparison is made using the developed model in conjunction with Chemkin II. The information utilized is the set of LLNL reaction rate data for light species interaction with other light species, the added rates of the unsteady light species due to the heavy species through the fitted KG_i and RL_i, and quasi-steady light molar densities through their curve-fitted mole fractions. An integral part of the *a posteriori* calculation is the computation of N_c from the fits for K_c according to eq. 3 and of the T evolution according to eq. 10 using the fits for K_h defined in eq. 13 and $C_{p,h}$ defined in eq. 12. Assessment of the reduced model involves comparison of its results with the equivalent results obtained using the full LLNL skeletal mechanism. This comparison is for $T(t), N_c(t)$ and $N_i(t)$.

The initial conditions specify ϕ, p_0 and T_0 which is slightly lower than T_s. Preliminary reduced model results indicated a strong sensitivity to initial conditions, particularly the value of T_s. This led to a further examination of the skeletal LLNL results near the initial conditions of the model calculations. This examination revealed that for an initial T rise of ~ 10 K, the rate of T increase is approximately linear with T; i.e. $dT/dt \triangleq K_0(T - T_{ap0})$ where T_{ap0} is the temperature (below T_0) at which dT/dt appears null, and where K_0 depends on T_s and ϕ. Comparison with the LLNL results shows that $K_0 = \nu_0 \phi^{0.1}(T_s/T_{ref})^{21}$ with $\nu_0 = 2.18 \times 10^{-5}$ s^{-1} and $T_s \triangleq T_0 + 12$ within a deviation of ~ 1 K. The reduced model was modified by using this initial rate for the region $\theta \lesssim 10^{-2}$, with a smooth transition at the larger θ just past 10^{-2} to the rate based on the energy equation involving the curve fit for K_h.

Results from the *a posteriori* evaluation using the modified reduced model are shown in Figs. 5-7. In all T evolution plots of Fig. 5 it can be seen that the temperature increase past an initial, quiescent region occurs too early compared to the LLNL results. This quiescent region is characterized by a small T rise ~ 5 K and nearly constant N_c, with almost no light species production. In a second, active part of the incubation region, T increases to ~ 1000 K, which results from the alteration of the structure of heavy radicals (i.e. their decomposition) the changes of which are represented by K_h through $\mathcal{R}_l$ of eq. 13 and by the corresponding enthalpies. The consequence of the T increase is a N_c decrease; light species begin to form during this time period. The time interval of this second region, which is also part of the incubation period, decreases with increasing p_0. The end of this second region is termed the ignition time. A successful model will predict both the ignition time and the end of the quiescent portion of the incubation region. Fig. 5 shows that

with the exception of the lowest pressure, $p_0 = 10$ bar, all the modified model simulations accurately recover this ignition time and the subsequent temperature rise, but none of them recovers the end of the quiescent incubation time which corresponds to $\theta \simeq 10^{-2}$. Following the small T jump from the quiescent to the active incubation region, θ becomes 10^{-1}; thus, it is apparent that modeling accuracy should be improved for $\theta < 10^{-2}$. With respect to the ignition time, the reduced model also shows a very sensitive dependency on T_s, with substantial changes in ignition times when T_s changes as little as 3 K. The conclusion is that although both LLNL results and our model shows this extreme sensitivity to T_s, the model in the $\theta \ll 1$ region does not accurately reproduce the LLNL results; this is because the current model does not address in enough detail the region $\theta = O(10^{-2})$, being based on a relatively sparse selection of LLNL results so as to minimize both the fitting effort and the eventual computational cost of the model. At this juncture, it is clear that additional modeling effort must be devoted to the quiescent incubation region. The splitting of the incubation region into the quiescent part followed by a pre-ignition T jump into a region of relatively slow T change - i.e. into the active incubation region - may be attributed to the form of the quasi-steady rate functions. These rates typically feature peaks at $\theta \lesssim 10^{-1}$, followed by a significant dip to a minimum, before an increase to the fast rate region. This rate fall-off coincides with the slow T rise in the active incubation region. The conjecture is that this general functional dependency is the essence of the Negative Temperature Coefficient (NTC) behavior.

Considering the molar densities illustrated in Figs. 6 and 7, the model qualitatively reproduces all of the timewise evolutions, but the quantitative agreement is only good to fair. The very good quantitative agreement of N_c versus θ of Fig. 6a hides the quantitative disagreement of N_c versus t of Fig. 6b. Although it would seem that this disagreement is due to an inaccurate K_c fit for $\theta \lesssim 10^{-2}$, the fact is that the discrepancy in the times of initial decrease of N_c (as shown in Fig. 6b) matches that of times in Fig. 5a at the end of the quiescent region. This explains the more favorable comparison in Fig. 6a which masks this discrepancy. Thus, the lack of quantitative $N_c(t)$ rendition of the LLNL results is traced to the necessity to generate a more accurate K_h fit in the $\theta = O(10^{-2})$ region, as already discussed in conjunction with the $T(t)$ variation. The need to capture this delay at the beginning of the active portion of the incubation region is also evident in the evolution of light species as a function of t depicted in Fig. 7.

VI. Conclusions

A computationally efficient kinetic reduction has been proposed for alkanes that has been illustrated for n-heptane using the LLNL heptane mechanism. The model is consistent with turbulence modeling in that scales were here first categorized into either those modeled or those computed as progress variables. Species were identified to be either light or heavy (C number $n \geqslant 3$). The heavy species were decomposed into defined 13 constituents and their total molar density was shown, through scrutiny of the LLNL mechanism, to evolve in a quasi-steady manner. The light species were shown through examination of the LLNL database to behave either in quasi-steady or unsteady manner. The modeled scales are the total constituent molar density rate evolution and the molar density of the quasi-steady light species. The progress variables are the total constituent molar density and the molar densities of the unsteady light species. The unsteady equations for the light species contain contributions of the type gain/loss rates from the heavy species that are modeled consistent with the developed mathematical forms for the total constituent molar density rate evolution since examination of these gain/loss rates shows that they also have a quasi-steady behavior with a functional form resembling that of the constituent rate. This finding highlights the fact that the fitting technique provides a methodology which can be repeatedly used to obtain an accurate representation of full or skeletal kinetic models.

An *a priori* study previously initiated was here completed with the development of mathematical functional forms for the quasi-steady light species and for the gain/loss rates for the unsteady light species. The proposed reduced model features 12 ultimate progress variables describing heptane oxidation. The reduced model requires fitting 16 quasi-steady rate functions, 11 curves for light quasi-steady mole fractions, and $C_{p,h}$. Also required are conventional rates between members of the light group, which are available in the literature. Some representative results of the functional forms were shown. Mathematically, the shown fits achieved substantial accuracy over seven rate decades considering the fact that they depend upon four variables.

The focus was here on the *a posteriori* study where the findings of the kinetically reduced mechanism were compared to corresponding results obtained from the LLNL database. The comparisons show that although

the model is qualitatively correct and reproduces the ignition time for the range of conditions investigated, more fine-tuning is necessary for the mathematical forms used in fitting the energetics of the constituents in a very small time interval near the simulation initiation in order to obtain better quantitative agreement with the LLNL results.

Assuming success with the modified reduced model, the advantage of the modeling approach is clear: Because this model is based on the N_c rate rather than on that of individual heavy species, even if the number of species increases with increased C number in the alkane group, providing that the quasi-steady rate aspect persists, then extension of this model to higher alkanes should be conceptually straightforward; although it remains to be seen if the functional fits would remain valid or would require reconstruction. Such a study is planned next by 'blindly' applying the n-heptane model to iso-octane and evaluate its predictions.

Acknowledgements

This study was conducted at the Jet Propulsion Laboratory (JPL), California Institute of Technology (Caltech) and sponsored at Caltech by the Army Research Office under the direction of Drs. David Mann, Kevin McNesby and Ralph Anthenien.

References

[1]Lawrence Livermore National Laboratory,http://www-cms.llnl.gov/combustion/combustion2.html.

[2]K. G. Harstad, J. Bellan 2008 A Simplified Model of Alkane Oxidation, AIAA 2008-0975, presented at the 46th Aerospace Sciences Meeting, Reno, NV, January 7-10, 2008.

[3]S. W. Benson, 1968 Thermochemical Kinetics., John Wiley & Sons, Inc..

[4]R. C. Reid, J. M. Prausnitz, B. E. Poling, 1987 The Properties of Gases and Liquids, McGraw-Hill Book Co., 4th edition, Chapt. 6.

[5]National Institute of Standards and Technology, Chemistry WebBook; http://webbook.nist.gov/chemistry/.

[6]CRC Handbook of Chemistry and Physics, 86th Ed., D. R. Lide, Ed.-in-chief, CRC Press, Boca Raton, Fl., 2005 (internet edition).

[7]Gas Research Institute, http://www.me.berkeley.edu/gri-mech/.

[8]NASA Glenn Research Center, http://cea.grc.nasa.gov/.

[9]T. Lu, C. K. Law, 2006 Linear time reduction of large kinetic mechanisms with directed relation graph: n-heptane and iso-octane, *Combust. Flame,* 144, 24-36.

[10]N. Peters, G. Paczko, R. Seiser, K. Sheshadri, 2002 Temperature cross-over and non-thermal runaway at two-stage ignition of n-heptane, *Combust. Flame,* 128, 38-59.

[11]V. I. Babushok, W. Tsang, 2004 Kinetic modeling of heptane combustion and PAH formation, *J. Propul. Power*, 20(3), 403-414.

[12]U. Maas, S. B. Pope, 1992, Simplifying chemical kinetics: intrinsic low-dimensional manifolds in composition space, *Combust. Flame*, 88, 239-264.

Mo/Ra	h^0	h^c	a^h	b^h
H_2	0.0	241.5	3.282	0.400
O_2	0.0	0.0	3.476	0.5663
N_2	0.0	0.0	3.388	0.469
C	717	1111	2.50	0.0
H_2O	-241.5	0.0	3.688	1.217
CO_2	-393.5	0.0	4.690	1.390
N	473	473	2.50	0.0
H	218.0	339	2.50	0.0
HO	38	159	3.385	0.3637
HOO	10.5	131	4.150	1.307
O	249.2	249.2	2.536	0.0
CO	-110.5	283	3.426	0.4749
HCO	43.1	558	4.154	1.2875
CH_4	-74.6	802	3.797	4.305
CH_3	146	902	4.440	2.249
CH_2	390	1025	3.973	1.3015
CH	596	1110	3.220	0.7136
C_2H_3	300	1449	5.1	3.5
HC_2	566	1474	4.434	1.404
C_2	838*	1625	4.58	0.0
NO	90.3	90.3	3.533	0.4508
NO_2	33.2	33.2	4.691	1.151
H_2O_2	-136	106	5.269	1.880
HCOH	-109	526.5	4.27	2.546
C_2H_2	228	1257	5.368	2.294
C_2H_4	52.5	1323	5.383	4.676

*Alternate value of 832 from the CRC tables.

Table 1. Thermodynamic properties of molecules and free radicals. h^0 and h^c (heats of formation and combustion, respectively), in kJ/mol; constants a^h and b^h for molar heat capacity in the form $C_p/R_u = a^h + b^h ln(T/T_{ref})$; T_{ref} = 298.15 K. "Mo" denotes "molecule". "Ra" denotes "radical".

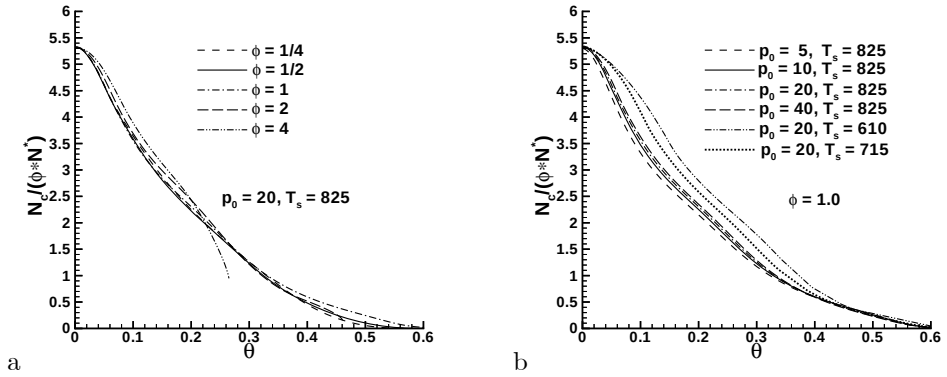

Figure 1. Similarity plots of parameter $N_c/(\phi \times N^*)$ versus θ at (a) $p_0 = 20$ bar and (b) $\phi = 1$ using the LLNL database. T_s is in K.

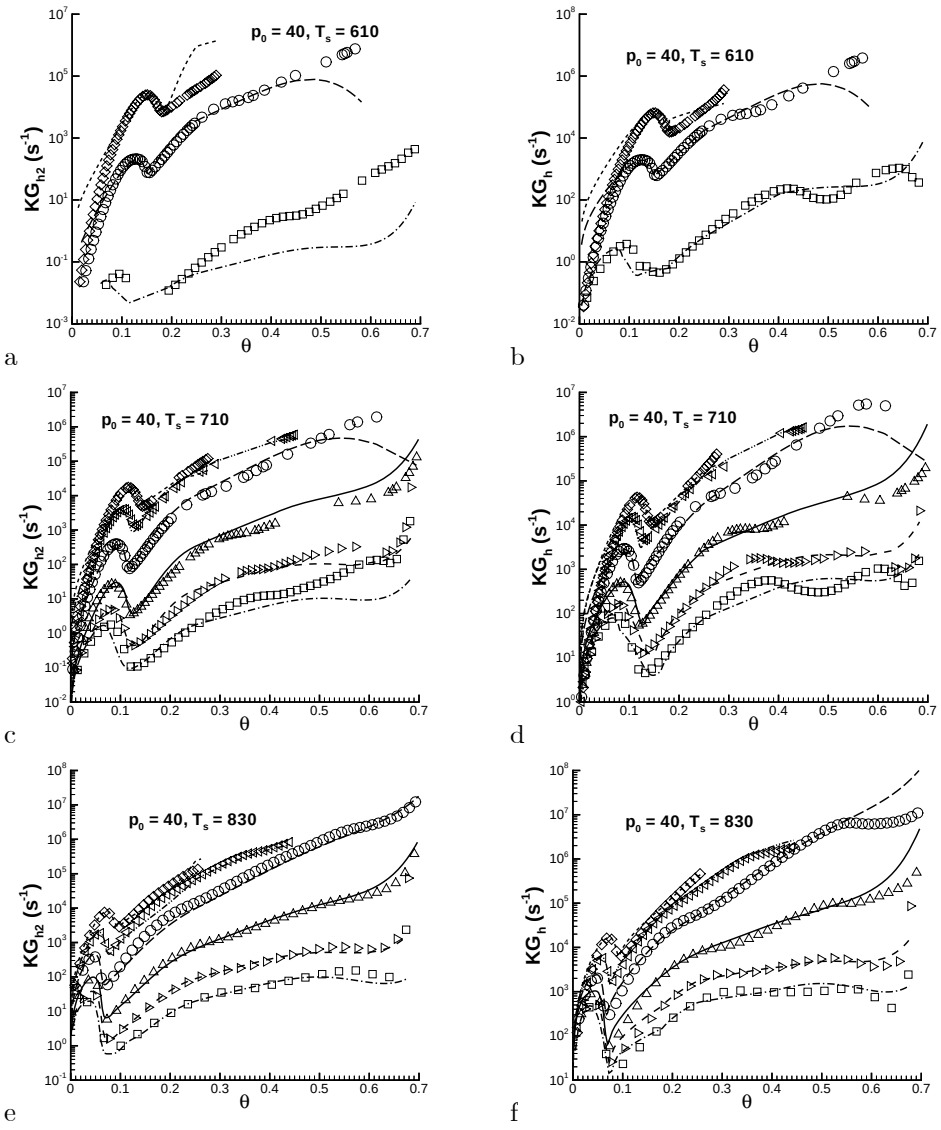

Figure 2. KG **versus** θ **for** $p_0 = 40$ **bar at different** T_s **values. Symbols** $\square, \triangleright, \Delta, \bigcirc, \triangleleft, \diamondsuit$ **represent selected results using the LLNL database; lines represent the corresponding fits. Temperatures units are in degrees K. The legend is:** $\square$, $-\bullet-\bullet-$ $\phi = 1/4$; $\triangleright$, - - - $\phi = 1/3$; Δ, —— $\phi = 1/2$; $\bigcirc$, $---$ $\phi = 1$; $\triangleleft$, $-\bullet\bullet-\bullet\bullet-$ $\phi = 2$; $\diamondsuit$, $\bullet\bullet\bullet$ $\phi = 4$. **(a,c,e) for** H_2 **and (b,d,f) for H.**

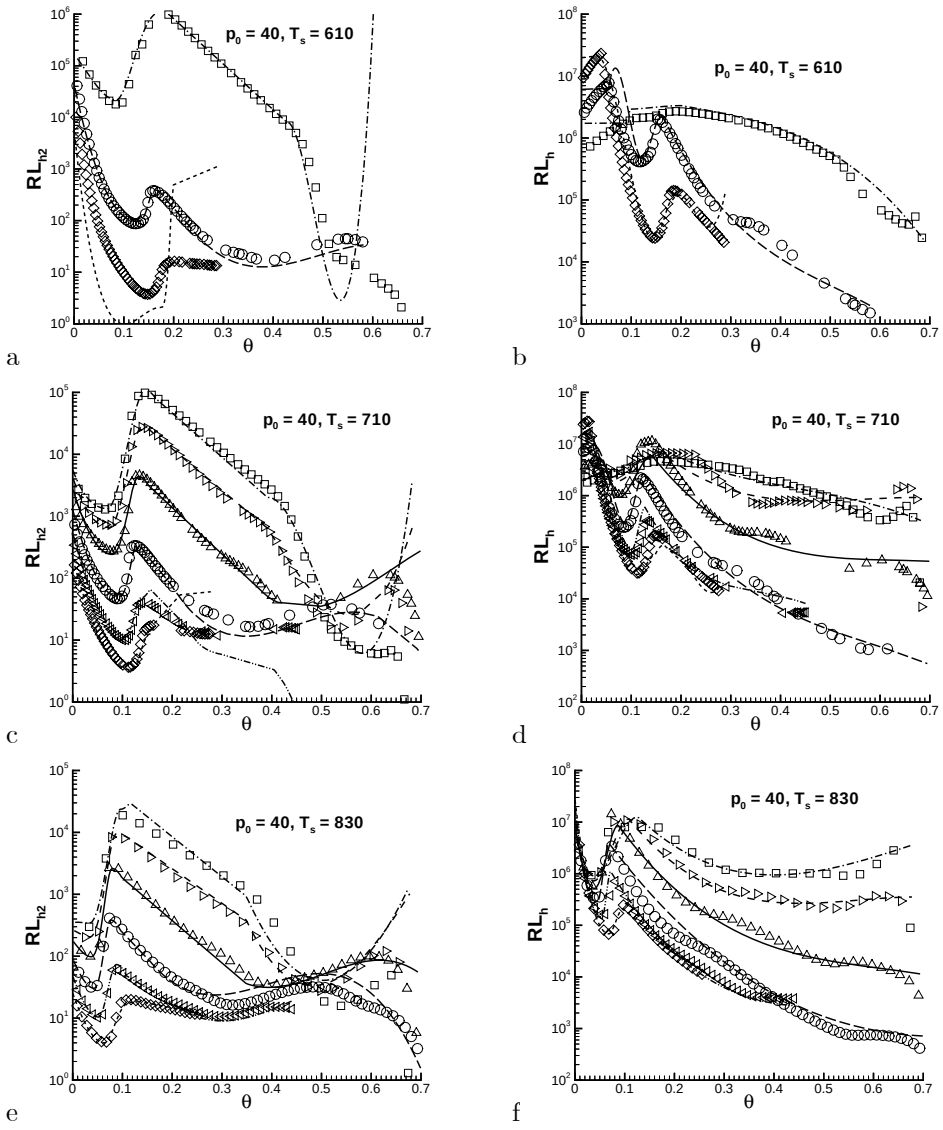

Figure 3. *RL* **versus** θ **for** $p_0 = 40$ **bar at different** T_s **values. Symbols** $\square, \triangleright, \Delta, \bigcirc, \triangleleft, \diamondsuit$ **represent selected results using the LLNL database; lines represent the corresponding fits. Temperatures units are in degrees K. The legend is:** $\square$, $-\bullet-\bullet-$ $\phi = 1/4$; $\triangleright$, - - - $\phi = 1/3$; Δ, —— $\phi = 1/2$; $\bigcirc$, $---$ $\phi = 1$; $\triangleleft$, $-\bullet\bullet-\bullet\bullet-$ $\phi = 2$; $\diamondsuit$, $\bullet\bullet\bullet$ $\phi = 4$. **(a,c,e) for** H_2 **and (b,d,f) for H.**

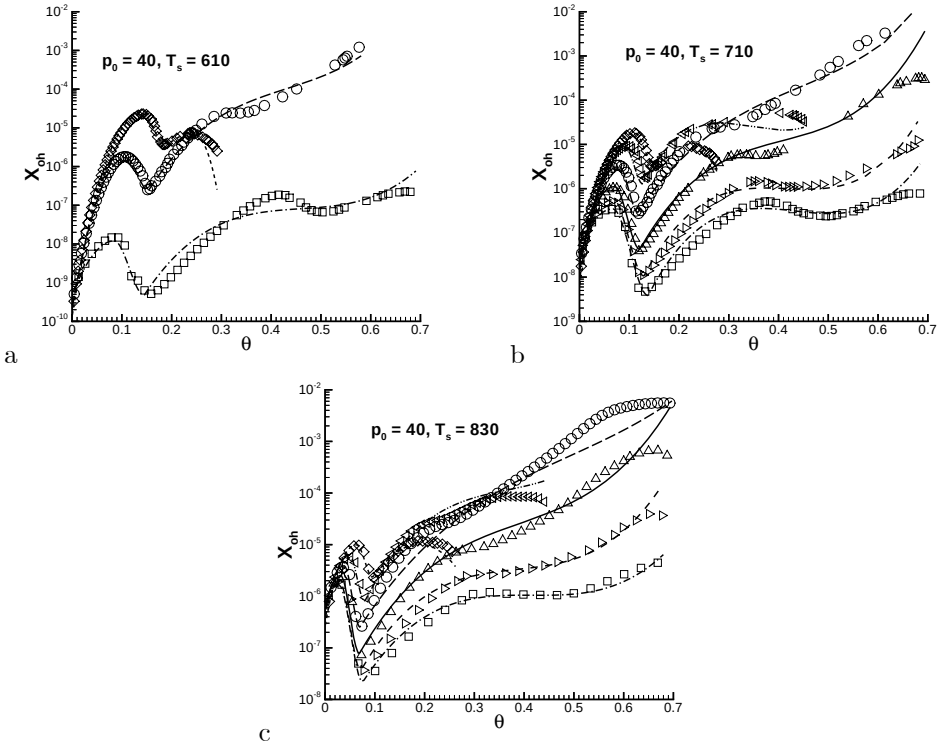

Figure 4. X_{OH} **versus** θ **for** $p_0 = 40$ **bar at different** T_s **values. Symbols** $\square, \triangleright, \Delta, \bigcirc, \triangleleft, \diamondsuit$ **represent selected results using the LLNL database; lines represent the corresponding fits. Temperatures units are in degrees K. The legend is:** $\square$, $-\bullet-\bullet-$ $\phi = 1/4$; $\triangleright$, **- - -** $\phi = 1/3$; Δ, —— $\phi = 1/2$; $\bigcirc$, $---$ $\phi = 1$; $\triangleleft$, $-\bullet\bullet-\bullet\bullet-$ $\phi = 2$; $\diamondsuit$, $\bullet\bullet\bullet$ $\phi = 4$.

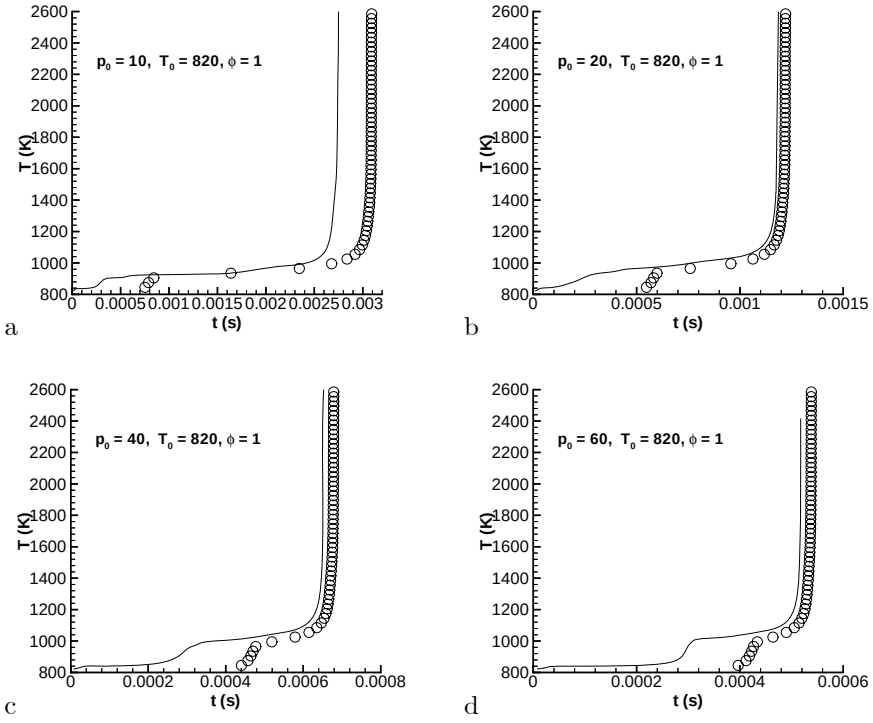

Figure 5. Timewise evolution of T **at** $\phi = 1$ **and** $T_0 = 820$ **K at several** p_0 **: (a) 10 bar, (b) 20 bar, (c) 40 bar and (d) 60 bar. The line is the model computation and the symbols are obtained using the LLNL database.**

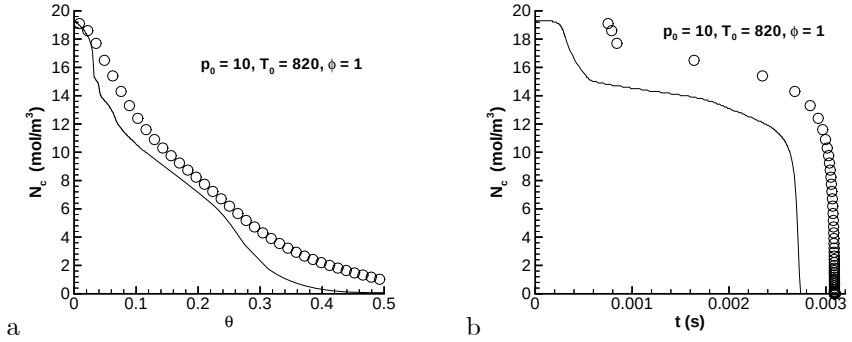

Figure 6. Evolution of N_c as a function of (a) θ and (b) t for $\phi = 1$, $p_0 = 10$ bar and $T_0 = 820$ K. The lines correspond to the model predictions and the symbols are obtained using the LLNL data.

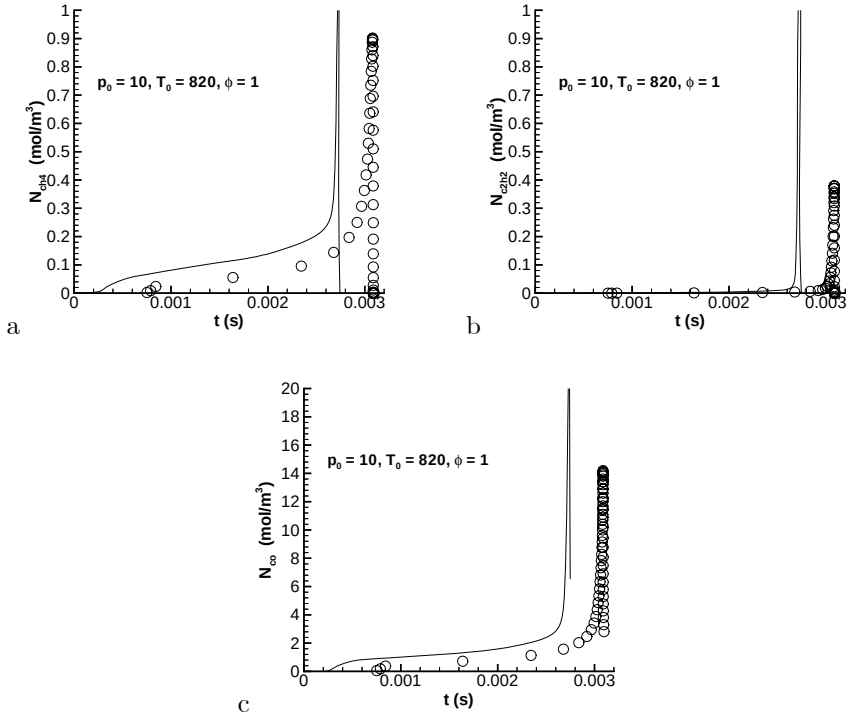

Figure 7. Timewise evolution of molar densities of several light species at $\phi = 1, p_0 = 10$ bar and $T_0 = 820$ K. (a) CH_4, (b) C_2H_2 and (c) CO. The lines correspond to the model predictions and the symbols are obtained using the LLNL data.